

SCALER: Versatile Multi-Limbed Robot for Free-Climbing in Extreme Terrains

Yusuke Tanaka¹, Yuki Shirai¹, Alexander Schperberg¹, Xuan Lin¹, and Dennis Hong¹

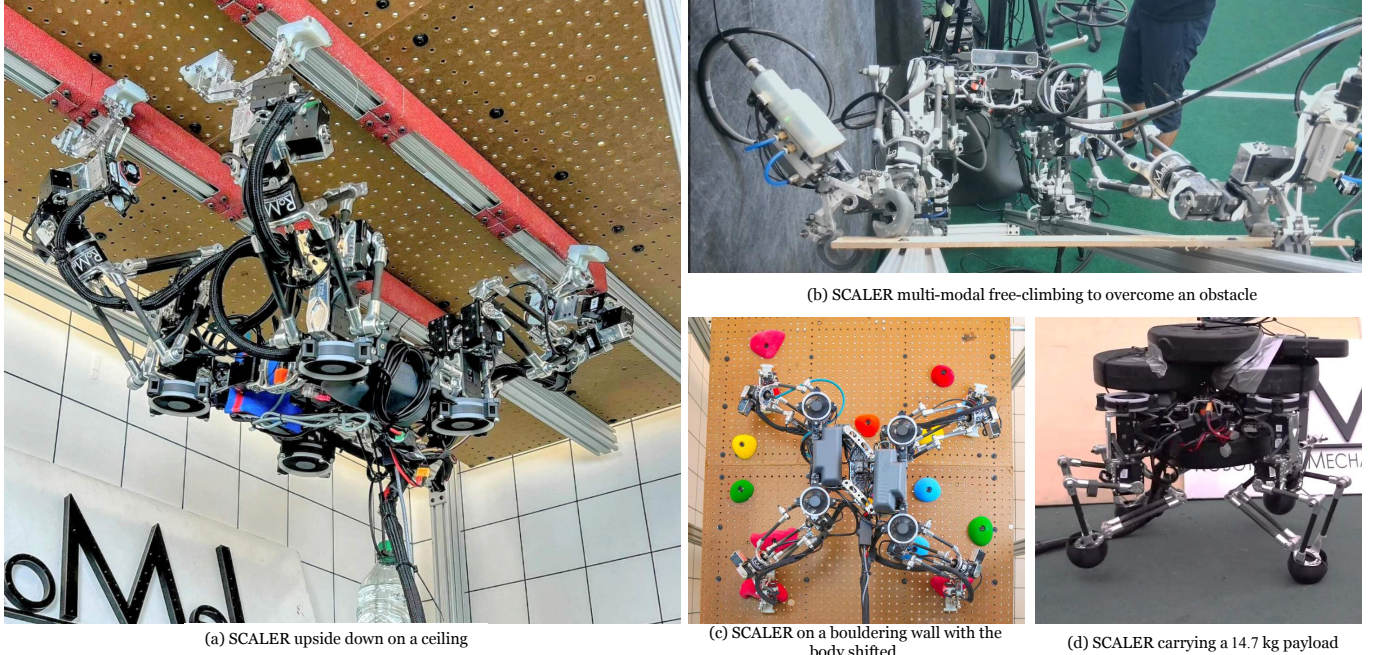


Fig. 1: SCALER, a versatile multi-limbed robot for free-climbing in extreme terrains.

Abstract—This paper presents SCALER, a versatile free-climbing multi-limbed robot that is designed to achieve tightly coupled simultaneous locomotion and dexterous grasping. Although existing quadruped-limbed robots have shown impressive dexterous skills such as object manipulation, it is essential to balance power-intensive locomotion and dexterous grasping capabilities. We design a torso linkage and a parallel-serial limb to meet such conflicting skills that pose unique challenges in the hardware designs. SCALER employs underactuated two-fingered GOAT grippers that can mechanically adapt and offer 7 modes of grasping, enabling SCALER to traverse extreme terrains with multi-modal grasping strategies. We study the whole-body approach, where SCALER uses its body and limbs to generate additional forces for stable grasping with environments, further enhancing versatility. Furthermore, we improve the GOAT gripper actuation speed to realize more dynamic climbing in a closed-loop control fashion. With these proposed technologies, SCALER can traverse vertical, overhang, upside-down, slippery terrains, and bouldering walls with non-convex-shaped climbing holds under the Earth’s gravity.

Index Terms—Climbing Robots, Grippers and Other End-Effectors, Legged Robots, Mechanism Design.

I. INTRODUCTION

The field of legged robotics set the stage for applications such as search and rescue, delivery, and even extraterrestrial

exploration [1]. They have shown versatility and maneuverability in locomotion [2] and have demonstrated contact-rich tasks such as object manipulation with their own body [3]. Limbed robots have further showcased grasping, using collective legs [4], utilizing a dedicated arm [5], or employing grasping end-effectors [6]. The simultaneous interaction between locomotion and grasping, called loco-grasping, allows them to execute tasks such as carrying objects, using tools, or traversing challenging terrains [7]. However, current locomotive robots are not yet sufficient to convey one of the extreme cases of loco-grasping, which is free-climbing [8], and it is essential for multi-limbed robots to facilitate even more versatile traversability over buildings, construction sites, or caves, etc. This includes the robots traversing over not only the continuous terrains defined in Fig. 2 but also discrete environments in Fig. 2b and directionally continuous in Fig. 2c.

However, achieving free-climbing raises substantial challenges. This domain mandates various climbing techniques and grasping adaptability as demonstrated in Fig. 1. Climbers have to consider foot placements and body stability [9], particularly in a discrete terrain environment such as in Fig. 2b. This imposes *strict* loco-grasping requirements; failure in either locomotion or grasping can result in a fall and task failure. Hence, free-climbing robots must consider closely coupled grasping and locomotion as illustrated in Fig. 3.

For tackling complex and cluttered terrains, performing

¹All authors are with the Department of Mechanical and Aerospace Engineering, University of California, Los Angeles, CA, USA 90095 {yusuketanaka, yukishirai4869, aschperberg28, maynight, dennishong}@ucla.edu.

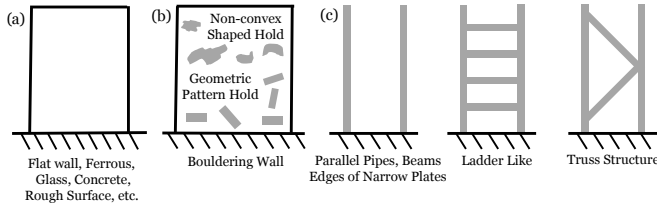


Fig. 2: The type of climbing environments in terms of their continuity. (a) a continuous environment. (b) a discrete environment. (c) directionally continuous environments.

multi-modal grasping becomes essential to improve climbing feasibility and stability. Multi-modal grasping is a cornerstone technique in human climbing to utilize various types of grips based on climbing scenarios [10]. Different grasping modes such as pinch, envelop, crimp, and pocket are strategically deployed to conquer terrains that would be otherwise difficult or impossible to travel [10], [11]. Whole-body approaches, such as the *sidepull* grasping technique [10], add a new set of potential abilities in climbing robots as they embrace the entire body and limbs to enhance grasping feasibility when holds are infeasible to grasp stably with one gripper. Therefore, free-climbing tasks must involve successful approaches and stable grips by switching among various grasping modes, depending on the environmental context and climbing requirement.

While existing platforms have paved the way for loco-grasping, there is still a gap in the strict loco-grasping and multi-modal ability in free-climbing. To address these challenges, we introduce SCALER: Spine-enhanced Climbing Autonomous Limbed Exploration Robot, a versatile quadruped-limbed research platform shown in Fig. 1. SCALER is designed to traverse a range of extreme surfaces. SCALER can cross obstacles using multi-modal grasping and whole-body approaches with our proposed unique C-shaped finger designs.

Our contributions are summarized as follows:

- 1) SCALER's Mechanisms: We propose SCALER torso and limb mechanisms for strictly coupled loco-grasping free-climbing. SCALER realizes versatile capabilities of traversing on the ground, vertical walls, overhangs, and ceilings with payload *under the Earth's gravity*.
- 2) Underactuated GOAT Grippers: We employ an improved mechanically adaptive GOAT gripper with spine tips.
- 3) Hardware Validation: We extensively validate the SCALER free-climber platform with the spine GOAT grippers in hardware experiments.

This paper extends our previous work [12] by introducing additional contributions related to dynamic locomotion and versatile climbing strategies, thereby advancing state-of-the-art robotic free-climbing.

- 1) Dynamic Climbing and Gait: We assess SCALER's capabilities during dynamic climbing with closed-loop control fashion and untethered operation. We introduce a modified trot gait to utilize limb stiffness and its model.
- 2) Multi-Modal Grasping with proposed grippers: We propose C-shaped finger GOAT grippers, (C-GOAT)s that can realize up to 7 modes of grasping with SCALER's dexterity. This capability enables SCALER to apply

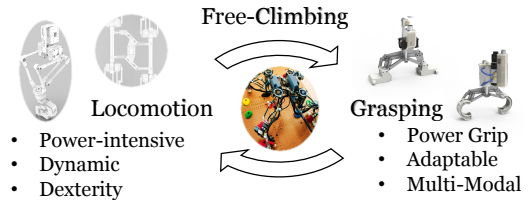


Fig. 3: The circular dependency diagram of the strict loco-grasping, free-climbing problem. SCALER requires a balance of both locomotion and grasping capabilities to achieve free-climbing.

versatile strategies, such as a whole-body approach to overcome - otherwise, it is infeasible to climb scenarios.

- 3) Analysis and Multi-Modal Climbing with C-GOAT: We analyze the C-GOAT characteristics and grasping capabilities in climbing tasks.
- 4) Hardware Validation: We validate SCALER dynamic gait and multi-modality in various hardware experiments.

To the best of our knowledge, SCALER is the first robot to demonstrate a versatile suite of free-climbing abilities under Earth's gravity, using more than two modes of grasping & conducting a whole-body approach in free-climbing. SCALER achieves this by combining SCALER's mechanical design and the GOAT grippers. Our approach makes SCALER a pioneering reference for future developments in robotic loco-grasping problems and free-climbing.

II. RELATED WORKS

In this section, we review the current state-of-the-art approaches in legged and climbing robotics, and climbing end-effector designs.

A. Quadruped Architecture

1) *Torso Mechanisms*: Torso mechanisms based on animal spines have been analyzed and validated for ground and climbing robots. Cheetah spine motions are implemented to improve locomotion efficiency by adding compliance in the body [13]. One degree of freedom (DoF) in the torso has demonstrated effectiveness in steering motions [14]. Inchworm gait extends and bends the body for a small soft robot to climb on a pole [15]. Slalom [16] replicated gecko in-plane bending movement, which reduced energy consumption in climbing by half compared to the rigid body on 30° slope. We introduce a new torso mechanism inspired by a human stretching motion when trying to reach a high object. This helps SCALER to climb in more restricted and contact-rich environments.

2) *Leg Mechanisms*: The latest quadruped robot technology utilizes quasi-direct drive torque actuators, such as those found in the MIT Cheetah [13], or series elastic actuators used in ANYmal [2]. While near-direct drive technology has proven successful on flat surfaces, it is not the most effective option for climbing, requiring continuous and intense power throughout the operation. One key difference between climbing and locomotion is that the robot must fight against gravity. Thus, the leg design sustains normal and shear forces under various gravity directions to support the robot [17].

LEMUR 3 is specialized for climbing under reduced gravity environments, which sacrifices locomotion speed and dynamic motion capability in exchange for rich continuous and holding torque provided by non-backdrivable 1:1200 gear ratio servo motors [18]. HubRobo has demonstrated bouldering free-climbing under 0.38 G using relatively high-gear ratio DC motors in serial [1], [19]. Parallel five-bar linkage mechanism legs used in Minitaur [20] and Doggo [21] are competent in dynamic motion and have high output force because two actuators' output power is linked. Bobcat [22] optimized the Minitaur link design for dynamic climbing. However, parallel linkage mechanisms increase complexity. When one robot operates on the ground, runs, climbs vertically, and grasps objects dexterously, balancing power density, speed, mechanical efficiency, and workspace simultaneously is crucial.

B. Climbing Robotics

Both wheeled [23] and linkage mechanism-based legged climbing robots [24] have successfully demonstrated climbing capabilities with spine-enhanced contacts for rock and concrete or with dry adhesive for clean flat surfaces, such as windows [25]. Soft robotics inspired by inchworm [15] or octopus [26] have replicated unique locomotion and grasping on a small scale. Inchworm style form factor legged robots have shown climbing over different climbing planes thanks to their high torso traversability [27]. A cable climber is intended for suspension bridge visual inspection [28]. While these robots have shown promising vertical climbing abilities, they employ fixed locomotion methods, making them unsuitable for versatile applications such as traversing complex and cluttered environments requiring various grasping strategies. In contrast, SCALER is designed to embrace its loco-grasping capability, allowing for versatile climbing techniques.

LEMUR 3 is a high DoF quadruped-limbed robot for space exploration missions [18]. HubRobo [1], [19] has reduced the hold grasping problem by employing a spine gripper that can passively grip a hold. However, neither can demonstrate free-climbing under the Earth's gravity.

Dynamic climbing necessitates robots with balanced holding torque and speed and end-effectors capable of rapid and reliable contact transitions [17]. RiSE [24] and Bobcat [22] can run on a vertical wall with spine crawl on rough concrete and a mesh surface, respectively. Marvel [17] has an electromagnetic foot that can dynamically climb on ferrous surfaces. These implicit and adhesive end effectors cannot consider dexterous contacts that are essential in the loco-grasping domain. SCALER focuses on loco-grasping in climbing, which is necessary to traverse discrete environments. SCALER uses pneumatically actuated grippers for dynamic climbing.

C. Climbing Contact Mechanisms

Grippers for climbing can be categorized based on the type of grasping mechanisms they employ, such as implicit adhesive methods or explicit grasping with fingers.

1) *Adhesive Contact:* For smooth surfaces, magnetic [17], [29], [27], [30] or suction-based [31], [32] end effectors, dry adhesive toes such as a gecko gripper [25], and Ethylene

Propylene Diene Monomer Rubber [16], are viable options for climbing robots. LEMUR 2B [18] and Capuchin [33] have demonstrated bouldering wall climbing with high-friction rubber-wrapped end-effector hooks, which let them hang onto the holds under the Earth's gravity. The pure frictional force is sufficient when a robot climbs between two walls [34]. For concrete, non-magnetic rough surfaces or loose cloth, spine-enhanced feet are desirable, such as in Spinybot II [35], CLASH [36], or the SiLVIA two-wall climber [37]. Spines or needles can get inserted into microcavities of rocky surfaces [1], [19]. With an array of spines, the gripper can grasp concave and convex shapes while collecting the environment geometries [38]. These implicit and adhesive types of contacts can reduce the loco-grasping problem in climbing tasks into just locomotion as long as they can stick to an environment.

2) *Finger Grasping Contact:* Two-fingered grippers have been utilized in climbing robotics such as ROMA I [11], which traverses truss structures, and Climbot [6], designed for vertical pole climbing and manipulation tasks. Humanoid robots have shown ladder climbing with grippers that hook or encompass the ladder step [9], [39]. LEMUR 3 and HubRobo consist of radially aligned micro-spines, supporting the robot weights under reduced gravity. A hand-shaped climbing gripper, SpinyHand [40], has four underactuated tendon-driven fingers that can switch between crimp and pinch grasping poses and has exhibited promising results for a human scale climbing robot. As free-climbing robotics communities study various grasping systems, selecting graspable locations correspondingly starts playing more important roles [41]–[44].

While these works show impressive grasping results in climbing, these systems still lack versatility and multi-modality in Section II-C3 that our gripper provides in SCALER. SCALER employs GOAT grippers [45], whippletree mechanism-based, passive underactuated two-fingered grippers that can mechanically adapt. Two variants of fingertips, spine, and dry adhesive are used in the GOAT grippers to address different scenarios.

3) *Multi-Modal Contact:* Multi-modal grasping, where more than one type of grasp can be realized based on the geometries of objects or tasks [46], is an effective method to improve the range of graspable objects. Multi-modal capable grippers consist of multiple DoFs and underactuation, such as the Robotiq 3-finger adaptive gripper, which has five grasp types [47]. Although these approaches are common in gripper communities, it is rare for climbing robots to use more than two grasping modes. SpinyHand [40] attempts to utilize multi-modality in climbing, but integration into the quadruped climbing robot is yet to be achieved.

Furthermore, a human climber can utilize their whole body to make difficult-to-grasp holds workable. This whole-body approach [10] can apply additional force on a hand to stabilize the grasp by using the whole-body to pull it. The whole-body approach can also increase frictional force, resulting in climbing on otherwise impossible terrains.

Our proposed C-GOAT gripper enables 7-modes grasping using only a single actuator. This adaptability sets SCALER apart from existing climbing robots and lets SCALER free-climb over obstacles while grasping them.

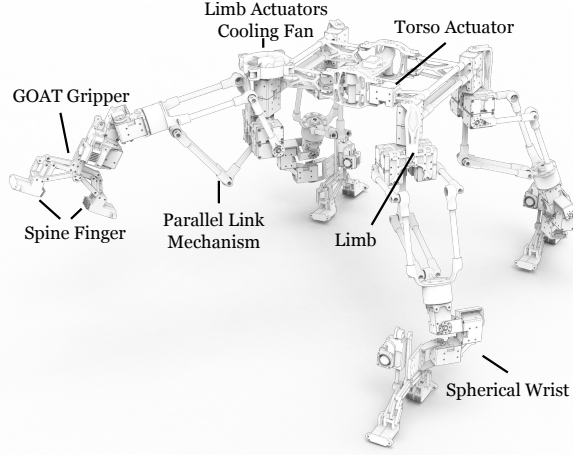


Fig. 4: SCALER isometric rendering view. SCALER is a four-limbed climbing robot with six-DoF legs, each featuring an underactuated GOAT gripper with one actuator. The torso actuator adds 1-DoF translation motion in the body.

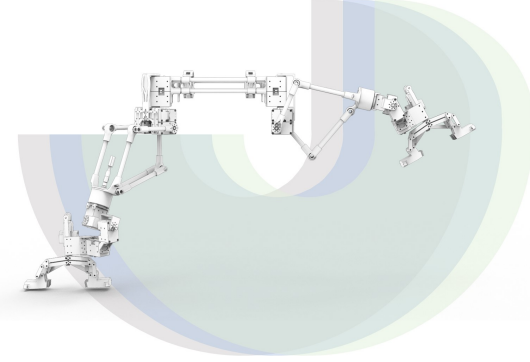


Fig. 5: SCALER 6-DoF limb workspace cross-section. The blue shadow area is the limb workspace with the nominal torso configuration, as shown in 6. The green and grey areas are when the torso is actuated $q_t = -45^\circ$ and $q_t = 45^\circ$, respectively, as shown in 6. The workspace excludes unreachable areas due to parallel link collisions, such as elbows with the body.

III. MECHANICAL DESIGN

SCALER in Fig. 1 and Fig. 4 is designed to achieve tightly coupled loco-grasping capabilities and meet power-intensive but dexterous operation requirements in climbing tasks while maintaining dynamic mobility. These specifications are accomplished with the following main components:

- The torso mechanism (Section III-A)
- The parallel-serial link limb (Section III-B)
- The gait designs (Section III-D)
- The mechanically adaptable GOAT gripper (Section IV)

A. Torso Mechanism

The SCALER body employs a four-bar linkage mechanism driven by one actuator, as illustrated in Fig. 6, which provides advantages in terms of workspace and forces. Conventional four-legged robots involving rigid one-body and having a torso DoF is less commonly adapted due to limited locomotion benefits than the complexity introduced. However, climbing robots can benefit from the additional DoF on the body, making the added complexity worthwhile. SCALER's torso includes a four-bar parallelogram linkage mechanism in Fig. 6,

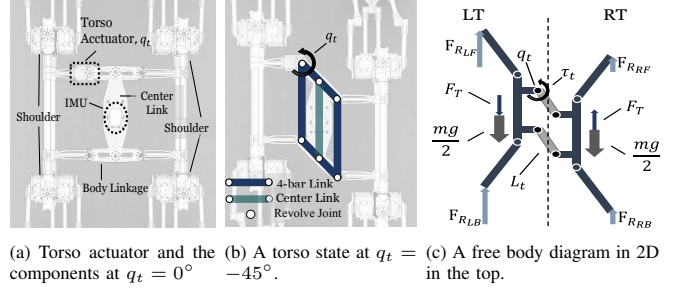


Fig. 6: The renderings and schematic of SCALER body and torso mechanisms from the top view.

which enables the robot to achieve more climbing strategies. Fig. 6a shows the torso's nominal condition and components. Fig. 6b illustrates the 4-bar linkage torso configurations when the torso actuator is at $q_t = -45^\circ$. The center link shown in Fig. 6a houses an IMU, battery compartments, and a computer, which allow the center of mass to be closer to constant regardless of the torso state. This mechanism particularly benefits SCALER in two ways: 1) Workspace advantages 2) Force advantages

In terms of workspace advantages, this mechanism can grant the potential to shift the robot workspace on demand, as a human can stretch their arm, such as when trying to reach high objects. The limb workspace shift is visualized in Fig. 5. This is demonstrated in the bouldering climb experiment in Section VI-D3. Furthermore, the translational torso motion can scale better to increase stride length than extending leg lengths since the limb workspace is spherical.

Regarding force advantages, the torso actuator generates a thrust force and reduces the load to lift the torso by half when climbing. The 2D free body diagram is in Fig. 6c, and the thrust force is calculated as $F_T = \tau_t / L_t$, where F_T is the thrust force, τ_t is the torque due to the q_t torso actuator, and the body linkage length, L_t . We compared the case where the torso is actuated and free-moving. One side of the body is rigidly fixed. When the torso is free moving, to pull up the half body, 44 N force was required. With the torso actuated, this reduced to 15 N, indicating 29 N thrusting in hardware.

B. Limb

In this section, we discuss SCALER's 6-DoF limb design and the design principles behind it as follows:

- 1) A redundantly actuated parallel linkage leg mechanism
- 2) The leg compliance modeling
- 3) Spherical wrist designs

Each limb of SCALER acts as both a supporting leg and a grasping arm when climbing. Thus, the leg design must account for locomotion and grasping capabilities.

1) *Redundantly Actuated Parallel-Serial Link Limb*: Climbing is power-intensive locomotion since the robots have to add potential energy and move against gravity. Hence, motor torque density and heat dissipation are critical. SCALER has to support and lift itself and withstand moments due to gravity that would otherwise pull SCALER off the wall. However, a very high-gear ratio, as seen in LEMUR 3 [18], sacrifices

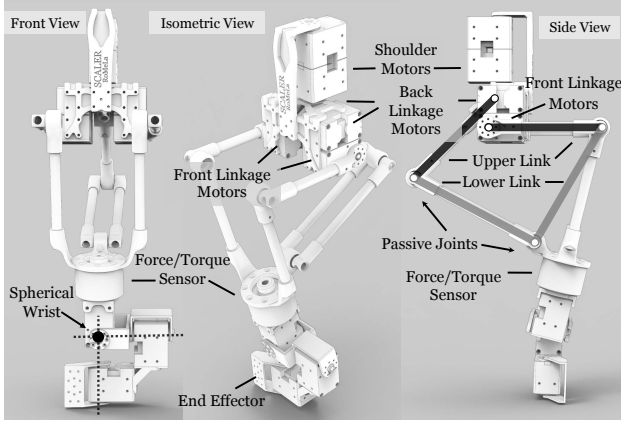


Fig. 7: SCALER 6-DoF limb. The side view shows the five-bar linkage kinematic design. The upper and lower links are in black and grey, respectively. The shoulder and five-bar linkages are driven by two motors each. The six-axis Force/Torque (F/T) sensor is installed at the end of the five-bar link, and the spherical wrist is on the sensor measurement face.

motion speed significantly, whereas quasi-direct drive motors are less suitable due to less continuous torque density and overheating. SCALER limb consists of a five-bar linkage, which is serially combined with a shoulder joint and a spherical wrist to attain 6-DoF per leg as illustrated in Fig. 7. SCALER limb workspace is visualized in Fig. 5. SCALER employs medium to high-gear ratio DC-servomotors, Dynamixel XM430-350 for all actuated joints.

The SCALER's five-bar parallel link mechanism utilizes two redundantly actuated joints to realize 2-DoF motions aligned in the climbing direction. The symmetric five-bar design is known to be mechanically superior in terms of proprioceptive sensitivity, force production, and thermal cost of force among serial and two different five-bar linkage leg designs in [20]. Although this choice of leg mechanism is ideal for power-intensive climbing operations, the parallel mechanism suffers from several modes of singularities that can happen in the middle of the workspace, such as where both front and back passive joints shown in Fig. 7 are at the same axis. In SCALER, this condition only happens outside the regular operation (e.g., when the end effector is inside the body) since the back linkage in Fig. 7 is marginally shorter. The passive elbow joints can make collisions with the environments or obstacles. However, it is uncommon for SCALER's climbing task since SCALER needs to raise the end effector high or the gripper to point, e.g., to the right as in Fig. 5.

In addition to the reduced thermal cost of force in the limb design, the coupled two motors at each joint distribute heat sources, keeping the motor temperature optimal and avoiding thermal throttling or damage. Such thermal considerations are vital since the power demands of free climbing are continuous. The detachable fan above the leg cools the shoulder-leg actuators in Fig. 4.

We compared the thermal performance of both the SCALER redundant motor configuration (two Dynamixel XM430-350 per joint) and a single but larger motor (Dynamixel XM540-150). We applied the same load and power. XM430-350 consumed 0.6 A per motor, and XM530-150 was 1.2 A at

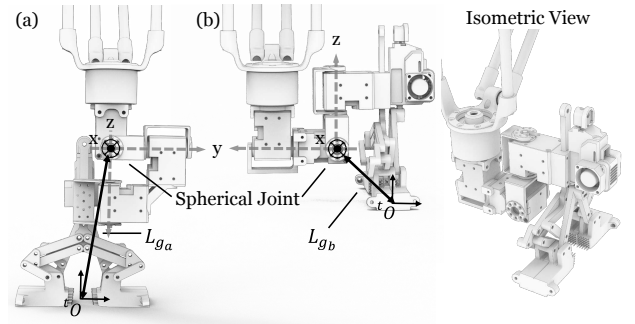


Fig. 8: SCALER 6-DoF spherical wrist variations. (a) Longer offset lengths can avoid gripper collision and have greater joint ranges. (b) Shorter and compact wrist but smaller effective range of motions. Their joint ranges and leg-to-wrist length ratios are in Table. I.

TABLE I: Wrist configurations and parameters.

Wrist Design	ζ	ϕ_x	ϕ_y	ϕ_z
Fig. 8a	30.0 %	$[-25, 90]^\circ$	$[-110, 110]^\circ$	$[-180, 90]^\circ$
Fig. 8b	15.2 %	$[-10, 90]^\circ$	$[-120, 120]^\circ$	$[-90, 90]^\circ$

The leg length is from the back linkage drive joint shown in Fig. 7 to the frame tO in Fig. 8, and the wrist length is from the spherical joint to the frame tO . The wrist and leg length ratio is $\zeta = \frac{L_{gj}}{L_l} \times 100$, where $L_{gj}, j \in \{a, b\}$ is the wrist Euclidean length from the spherical joint to the fingertip frame, tO in Fig. 8. L_l is the leg Euclidean length from the leg back linkage motor joint in Fig. 7 to tO .

13.8 V. The output torque difference was 5 %. the SCALER's motor configuration case saturated to 48.5 °C with a time constant 9.8 minutes. Over 1 hour of testing, the SCALER motor configuration did not overheat. On the other hand, the single larger motor temperature quickly raised to 50 °C after 16 minutes. It was predicted to saturate at 57 °C, but it would have damaged the motor, and we had to terminate the test. This indicates that having the redundant motors per joint, as in SCALER, is thermally advantageous.

The weight of SCALER's limb is distributed on both ends: the body and the wrist. The intermediate links are structured with carbon fiber tubes. When the wrist and grippers are not installed, the leg consists of relatively low inertia, improving the swing leg dynamics.

2) *Limb Compliance Modeling*: The Virtual Joint Method (VJM) modeling [49] is used to approximate limb stiffness. This model is verified through experiments in Section VI-A4. The model is based on lumped modeling and assumes joint stiffness as linear springs for small angles with a rigid link [49]. The VJM stiffness model is necessary for stiffness force control and estimation in climbing tasks as demonstrated in [34]. The model considers the shoulder and the parallel mechanisms, and the compliance in the metal wrist and gripper linkages is negligible compared to these parts.

The stiffness matrix for SCALER's parallel-serial leg is formulated as follows:

$$K = \left(\frac{1}{k_0} + \frac{1}{k_1 + k_2} \right)^{-1} J^\top J \quad (1)$$

Where K is a stiffness matrix in the Cartesian coordinate, k_0, k_1, k_2 are joint stiffness at the shoulder and two parallel linkage drive joints shown in Fig. 7, and J is a $\mathbb{R}^{3 \times 3}$

TABLE II: SCALER configuration list.

Configuration	Limb DoF	Wrist	GOAT Actuator (Section IV-B)	GOAT Finger (Section IV-C)	Applications	Fig.	Experiments Section
Walking	3	N/A	N/A	N/A	Ground Locomotion	1b 9a	VI-A1, VI-B1
Spine Climbing	6	Fig. 8a	DC Linear	Spine Cell	Climbing on Rough Surfaces	1a,c, 4	VI-C, VI-B2, VI-D3
Dynamic/Multi-Modal Climbing	6	Fig. 8b	Pneumatic	C-Shaped Dry Adhesive	Dynamic Multi-Modal Climbing Slippery Terrain	1d	VI-A2, VI-D1, VI-D2
Bi-Manipulator	6	Fig. 8a	N/A	N/A	Fixed-Base Manipulation	9b	VI-C in [48]

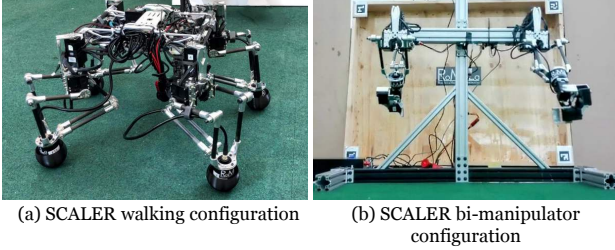


Fig. 9: Different configurations of SCALER.

Jacobian matrix for the leg excluding spherical joints. The condition number, κ indicates relative stiffness at a specific joint configuration, and it is obtained from (2):

$$\frac{1}{\kappa} = \sqrt{\frac{\lambda_{\min}}{\lambda_{\max}}} \quad (2)$$

λ_{\min} and λ_{\max} are the minimum and maximum eigenvalues of the stiffness matrix, K . The stiffness map obtained from the hardware is in Section VI-A4.

3) *Spherical Wrist*: The spherical wrist design contributes to the robot's workspace since free-climbing requires dexterity. SCALER employs spherical wrists as shown in Fig. 7 and Fig. 8, which have uniform end-effector offsets for all rotations and simpler inverse kinematics. Two SCALER wrist designs are shown in Fig. 8 and detailed in Table I. While the added wrist length helps prevent wrist collisions with the environment, it also limits reachability and raises torque needs at leg joints. The wrist in Fig. 8a used in [12] occupies 30 % of the limb length, whereas the wrist Fig. 8b is 15 %.

C. Modularity

SCALER design incorporates modularity, enhancing its applications for different objectives and research. This section explores various SCALER configurations and modules.

1) *SCALER Configurations*: Modularity provides both engineering benefits and additional capabilities beyond climbing, as shown in Fig. 9. Primary SCALER configurations are listed in Table II. SCALER's climbing configurations include four 6-DoF limbs and a 1-DoF torso, resulting in 25-DoF. Each limb includes a two-fingered underactuated 2-DoF gripper driven by one actuator, as detailed in Section IV.

The walking configuration in Fig. 9a has 3-DoF per leg by replacing the spherical wrist with a flexible semi-spherical foot cover to protect the force/torque (F/T) sensor. The walking format benefits from the minimal inertia design of SCALER's parallel linkage leg. A bimanual manipulator configuration uses two SCALER limbs attached on a fixed base as shown in Fig. 9b and is experimented with in [48].

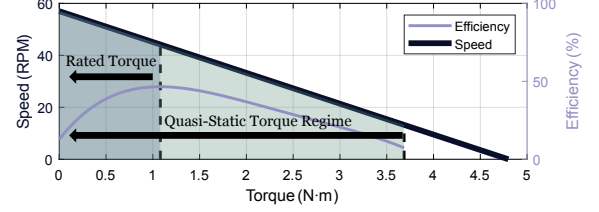


Fig. 10: Torque-speed curve for the servo motor used in SCALER at 14.8 V.

2) *Untethered Operation Modules*: For untethered operations, SCALER is equipped with additional computing and power modules. The PC and battery can be latched on the top and bottom of the center link in Fig. 6, respectively. A Jetson Orin unit weighing 0.97 kg is employed for onboard vision and multi-depth camera processing, whereas a NUC6i5SYK unit weighing 0.39 kg is used for non-GPU intensive applications. Power modules comprise a MaxAmp 4S 14.8 V, 8000 or 12000 mAh Li-Po battery, paired with DC-DC converters with a wireless emergency stop. The gripper is connected via M12 cables, and the pneumatic system described in Section IV-B requires additional CO₂ gas tanks with a regulator on the body.

D. SCALER Gait

In this section, we introduce two new climbing gaits utilizing SCALER's torso mechanism and limb stiffness.

- 1) SKATE Gait
- 2) Modified Trot Gait

These gaits benefit SCALER by taking advantage of its mechanical intelligence. The SKATE gait ensures quasi-static climbing by having two limbs always stationary, whereas the modified trot gait is meant for tasks where force control is critical, such as dynamic climbing.

1) *SKATE Gait*: SCALER's torso mechanism allows a unique gait called the Shifting Kinematics Adaptive Torso Extension (SKATE) gait. Our SKATE gait uses the torso actuation to maximize the advantage of the thrust force as described in Section III-A. The main benefit of this SKATE gait is that half side of the body is always stationary, which utilizes the quasi-static regime of the motor torque as visualized in Fig. 10. This is a common approach in high gear ratio actuators [50] at the cost of efficiency as in Fig. 10. In the SKATE gait, only half of the body moves forward for one motion sequence, such as the Right Torso (RT), and then the Left Torso (LT) moves forward. The gait legend and SKATE gait schedule are shown in Fig. 11 and Fig. 12a. The RT lift sequence uses the Right Front (RF) and the Right Back (RB) legs as follows:

- 1) **Phase 0**: Swing the RF leg.
- 2) **Phase 1**: Lift RT with RF, RB, and the torso actuator.

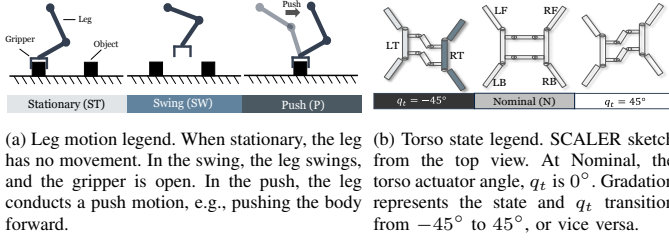


Fig. 11: Leg and torso state legends for gait schedules in Fig. 12 and Fig. 13.

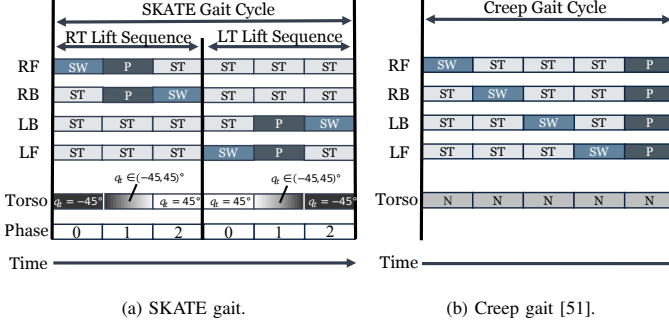


Fig. 12: SKATE gait and creep gait schedules comparisons. The SKATE gait phases are defined in Section III-D1. Leg and torso state legends are in Fig. 11.

3) Phase 2: Swing the RB leg.

While RT is in this lift sequence, the LT, the other side of the body, the Left Front (LF), and the Left Back (LB) legs are stationary, meaning they are not in motion. During **Phase 1**, the torso actuator rotates from $q_t = -45^\circ$ to $q_t = 45^\circ$. After **Phase 2**, LT enters the lift sequence, which repeats the same pattern. RT is stationary instead.

- 1) **Phase 0**: Swing the LF leg.
- 2) **Phase 1**: Lift LT with LF, LB, and the torso actuator.
- 3) **Phase 2**: Swing the LB leg.

Thus, SCALER alternately lifts RT and LT over the cycle of the SKATE gait. The leg actuators can tolerate higher holding torque than in continuous motion as in Fig. 10. Furthermore, the swing legs are assisted by the thrust force from the torso actuator as illustrated in Fig. 6c. Compared to the creep gait in Fig. 12b, the SKATE gait has two body lift phases, and at least two legs are always stationary.

2) **Modified Trot Gait Sequence**: Dynamic climbing presents unique challenges, notably the sag-down effect. This effect arises from a combination of gravity, angular slips around the gripping points, and inherent mechanical compliance. To address this problem, we propose a modified trot gait sequence that has a dedicated stiffness force control pushing phase, and the gait schedule is shown in Fig. 13a.

The sequence unfolds over three phases:

- 1) **Phase A**: A pushing action switches the support force from the RF/LB to the RB/LF leg pair. After this phase, the RB/LF leg pair primarily supports SCALER's weight.
- 2) **Phase B**: The RF/LB grippers open and swing forward.
- 3) **Phase C**: The RF/LB grippers re-engage, resulting in a four-leg stance.

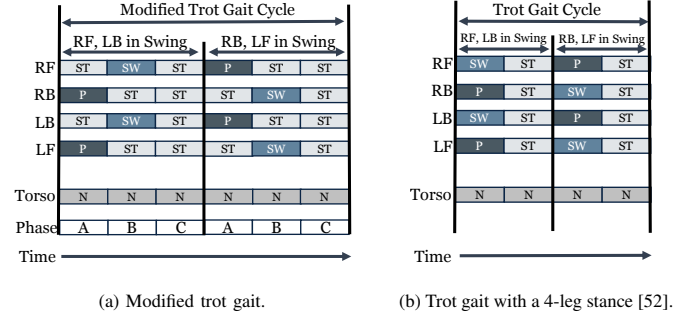


Fig. 13: Modified trot gait and trot gait with a 4-leg stance schedules comparisons. The modified trot gait phases are defined in Section III-D2. Leg and torso state legends are in Fig. 11.

Compared to a conventional trot gait with a 4-leg stance presented in Fig. 13b, the benefits of using this modified trot gait in climbing are by adding a dedicated push phase, **Phase A** in Fig. 13a. It minimizes the change in supporting forces when the diagonal leg pair switches at the beginning of **Phase B**. This approach ensures a smooth and controlled transfer of supporting forces between trot leg pairs and reduces abrupt changes in support force distribution. A four-leg stance enhances gait stability, as argued in [52]. We demonstrate this modified trot gait in Section VI-A2 and evaluate its performance in Section VI-A3, along with the associated mechanical stiffness in Section VI-A4.

IV. GOAT GRIPPER

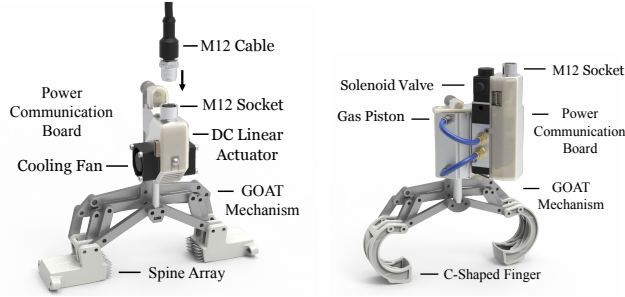
In the following section, we present the GOAT gripper [45], a mechanically adaptable underactuated gripper. First, we outline the principles of the GOAT mechanism and its inherent capability in climbing environments. Then, we describe two distinct modules of the gripper as follows:

- DC linear actuator spine GOAT grippers in Fig. 14a.
- Compressed gas pneumatic GOAT grippers with C-shaped fingers: C-GOAT in Fig. 14b.

The spine-enhanced fingertips are adequate on rough surfaces discussed in Section IV-C1, and the C-shaped fingertips can realize multi-modal grasping as detailed in Section IV-D, thereby illustrating their versatility in addressing diverse climbing challenges.

A. The GOAT Mechanism

Here, we introduce the GOAT mechanism [45] visualized in Fig. 15a, which is used in SCALER's GOAT grippers. The GOAT mechanism is a mechanically adaptable whiplike-based underactuated rigid linkage system. Successful free-climbing in discrete environments requires grasping holds despite various uncertainties. The GOAT gripper can help mitigate these challenges by compensating for end-effector configuration errors with one passive DoF. Traditional parallel jaw grippers have only 1-DoF, either open or closed, and grasp objects at their central axis. The GOAT's extra underactuation allows the GOAT gripper to adapt passively and grasp off-center objects as is, as illustrated in Fig. 15a. This adaptability



(a) The GOAT gripper with a DC linear actuator and spine arrays. (b) The C-GOAT rendered image. The fingers are covered with dry adhesive.

Fig. 14: Two variants of GOAT grippers.

is further extended to realize multiple modes of grasping, as detailed in Section IV-D.

During the design process of the GOAT gripper, the linkage lengths, workspace, and forces are parametrically optimized, as discussed in [45]. The design process considered bouldering hold sizes and the force requirements necessary to support SCALER's weight. This formed a multi-objective nonlinear optimization problem with two objectives: two fingertips with active and passive DoF motion ranges and fingertip normal forces based on static force equilibrium. These two objectives are in a trade-off relationship, and the optimized GOAT mechanism is evaluated with bouldering holds in [45]. Since the optimization uses a 2D minimum bounding box, objects that meet this assumption and are in the size range are already considered, such as aluminum structures shown in Fig. 1.

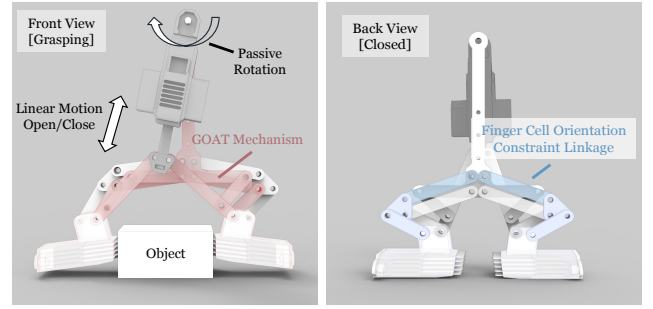
In contrast to the design in [45], the external four-bar linkages constrain the orientations of the fingertip to remain parallel to each other, as shown in Fig. 16, 15b. This constraint ensures that the fingertip contact surface, such as the angle of the spine needles, remains constant regardless of the GOAT gripper's kinematics configurations, as shown in Fig. 16b, 16c. The parallelogram mechanism linkages do not affect the gripper kinematics or optimization results. The parallelogram linkage length are trivial since they should be equal to the GOAT mechanisms linkage in parallel.

B. Gripper Actuation

Here, we discuss two actuators used in our GOAT gripper:

- A DC linear actuator (Fig. 14a)
- A CO₂ high-pressure pneumatic actuator (Fig. 14b)

While lightweight and capable of closed-loop controls, the DC linear actuators rendered in Fig. 14a operate at a slower speed, which motivated us to employ a faster actuation. With the DC linear actuator, the GOAT grippers open and close fully at a frequency of 0.12 Hz with no load. In contrast, the high-pressure pneumatic actuator shown in Fig. 14b can run at a frequency of 5 Hz. Additional gas tanks and regulators are installed on the SCALER's body. The DC linear actuator is rated at 100 N continuous output and the maximum 200 N. The pneumatic actuator can output the maximum 310 N force at 1 MPa, but nominal is 200 N at 0.65 MPa. The higher force is necessary for C-GOAT since the friction coefficient is lower than the spine. Consequently, the pneumatic-driven



(a) The GOAT gripper, when grasping at the off-axis. The GOAT mechanism [45] is visualized in red. (b) GOAT grippers when closed. The fingertip off-axis. The GOAT mechanism [45] is visualized in red.

Fig. 15: The GOAT mechanism and linkages.

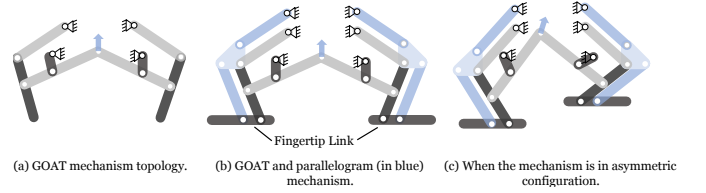


Fig. 16: The topology of the GOAT mechanism and the additional parallelogram mechanism constraining the fingertip orientations constant. The linkage lengths and configurations are non-optimal for visualization purposes.

GOAT gripper allows SCALER to climb faster, albeit at the cost of SCALER's payload due to additional components and the lack of sensors compared to the DC linear actuator.

C. GOAT Gripper Fingertip

GOAT grippers have two types of fingers depending on the surface and applications as follows:

- 1) Spring-Loaded Spine Enhanced Fingers
- 2) C-shaped Dry Adhesive Enhanced Fingers

The spine tips are for rough and rocky surfaces, whereas the dry adhesive can grasp slippery terrains.

1) *Spring-Loaded Spine-Enhanced Fingers*: The spring-loaded spine-enhanced finger GOAT gripper is rendered in Fig. 14a. Our spine cell design is based on [53]. Each cell comprises fifty spines, each with a diameter of \varnothing 0.93 mm, and a 5 mN/mm spring. The cell surface is slanted so that the spines approach at an optimal angle. Strain gauges can measure normal-axis fingertip force, as demonstrated in [54]. The spine tips are more appropriate on textured and rough surfaces, such as rock, concrete, and bouldering holds with microcavities on their surface [38].

2) *C-shaped Dry Adhesive Enhanced Fingers*: The C-GOAT gripper shown in Fig. 14b can realize seven different grasping modes by utilizing both actuated and underactuated DoFs, and the robot's whole body as shown in Fig. 17. Because of finger geometries, the C-shaped finger has an elastomer dry adhesive applied to both the inside and outside C sections instead of spine arrays. The dry adhesive increases the friction coefficient, and thus, the robot can climb slippery terrains.

D. Multi-Modal Grasping with C-GOAT

1) *GOAT Gripper Multi-Modality*: Diverse grasping modes allow robots to use an appropriate type of grasping method for

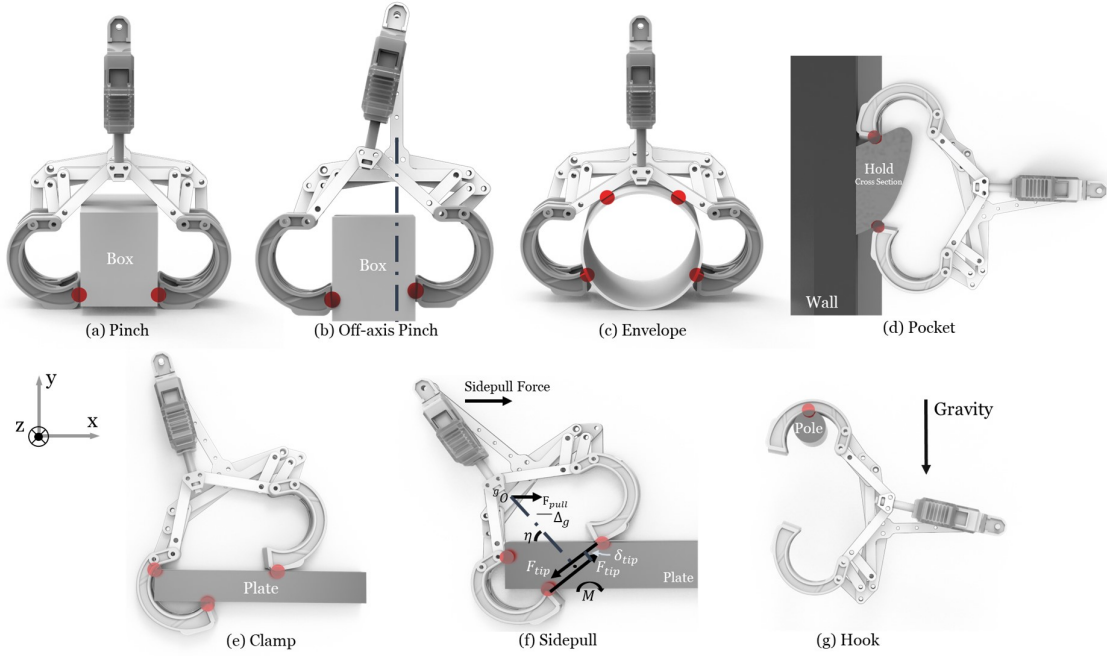


Fig. 17: C-GOAT gripper's 7 different grasping modes. Red dots represent primary points of contact that render grasping forces.

TABLE III: Type of grasping modes and their characteristics

Mode	Objects	Figure
Pinch	General Items in the range	17a
Pinch Off-axis	Items placed off-centered	17b
Envelop	Cylindrical items	17c
Clamp	Plates thinner than the C-finger opening	17f
Sidepull	Plates thicker than the C-finger opening	17g
Pocket	Items with pocket holes larger than fingertips	17d
Hook	Bars and pipes smaller than C-finger	17g

TABLE IV: Grasping Mode Contact Characteristics

	\hat{x}^+	\hat{x}^-	\hat{y}^+	\hat{y}^-	\hat{z}^+	\hat{z}^-
Pinch	0	0	†	†	†	†
Pinch off-axis	0	0	‡	‡	‡	‡
Envelop	0	0	‡‡	0	‡‡	‡‡
Clamp	0	§	0	0	§	§
Sidepull	*	§	0	0	§	§
Pocket	0	0	0	0	†	†
Hook / Encompass	0	$\in \mathbb{R}$	0	0	$\in \mathbb{R}$	$\in \mathbb{R}$

Given $\eta := \{x, y, z\}$, $\dot{\eta} = \dot{\eta}^+ - \dot{\eta}^-$, $(\dot{\eta}^+, \dot{\eta}^- \geq 0)$. $\dot{\eta}^+ = 0$ or $\dot{\eta}^- = 0$ implies no motion due to physical constraints in that respective direction. \mathcal{Q}_p , \mathcal{Q}_{po} , \mathcal{Q}_e , \mathcal{Q}_c are the limit surface of the pinch, pinch off-axis, envelope, and clamp, respectively, in Fig. 18. †: 0 if $F \in \mathcal{Q}_p$. ‡: 0 if $F \in \mathcal{Q}_{po}$. ‡‡: 0 if $F \in \mathcal{Q}_e$. §: 0 if $F \in \mathcal{Q}_c$. *: 0 if $F > F_{\text{sidepull}}$. Unrestricted if $\in \mathbb{R}$.

different geometries. Paired with C-shaped fingers and one underactuated DoF, SCALER can embrace the potential for versatile and dexterous multi-modal grasp in climbing. The list of modes and applicable objects is listed in Table III.

Pinch and envelope grasps [47] are standard in two-fingered grippers rendered in Fig. 17a,c, respectively. The pinch grasp relies more on friction, while the envelope encompasses an object mechanically, adding more kinematic constraints. Thanks to GOAT gripper's underactuated, it can pinch grasp an object off-center axis as in Fig. 17b.

The plate clamp in Fig. 17e resembles a crimp grip, and it

allows the GOAT gripper to clamp down thin plates with the C-shaped fingers and underactuation. When encountering plates with a thickness beyond the C-shaped opening, SCALER can embrace a whole-body approach, *sidepull*, to stabilize the grasping instead. This tactic is common for a human climber to overcome bouldering holds that cannot be grasped [10]. SCALER can pull the gripper to the side in Fig. 17f, which ensures the third inner contact point occurs, adding physical constraint.

Pocket grasp [10], and hook [11] allow SCALER to hook onto narrow structures, such as large cavity, poles and wire, as shown in Fig. 17d,g. These methods have more physical constraints and less reliance on fictional forces. Pocket grasp can generate a grasping force due to the gripper actuator, whereas hook cannot and solely relies on kinematic constraints or external forces.

Demonstrations of multi-modal grasping are explored in Section VI-D1 and VI-D2.

2) *Sidepull Force Requirements*: The fingertip's normal force will generate a moment when grasping a thick plate. Hence, the sidepull force must cause at least a greater moment as in (3) and parameters visualized in Fig. 17f.

$$\left\{ F_{\text{tip}}, F_{\text{pull}} \left| \begin{array}{l} \sum \mathcal{M} = \delta_{\text{tip}} F_{\text{tip}} + \Delta_g F_{\text{pull}} \sin \eta \geq 0, \\ F_{\text{tip}} \in \mathcal{Q}_{\text{limit}}, \end{array} \right. \right\} \quad (3)$$

Here, \mathcal{M} is a moment acting due to the fingertip force vectors denoted as F_{tip} . δ_{tip} is the Euclidean distance between two F_{tip} , F_{tip} . Δ_g is the perpendicular distance from the center of grasp and the gripper frame, F_{pull} is the sidepull force, and η is the gripper angle with respect to the plate grasping. The sidepull whole-body technique is experimented with in Section VI-D2.

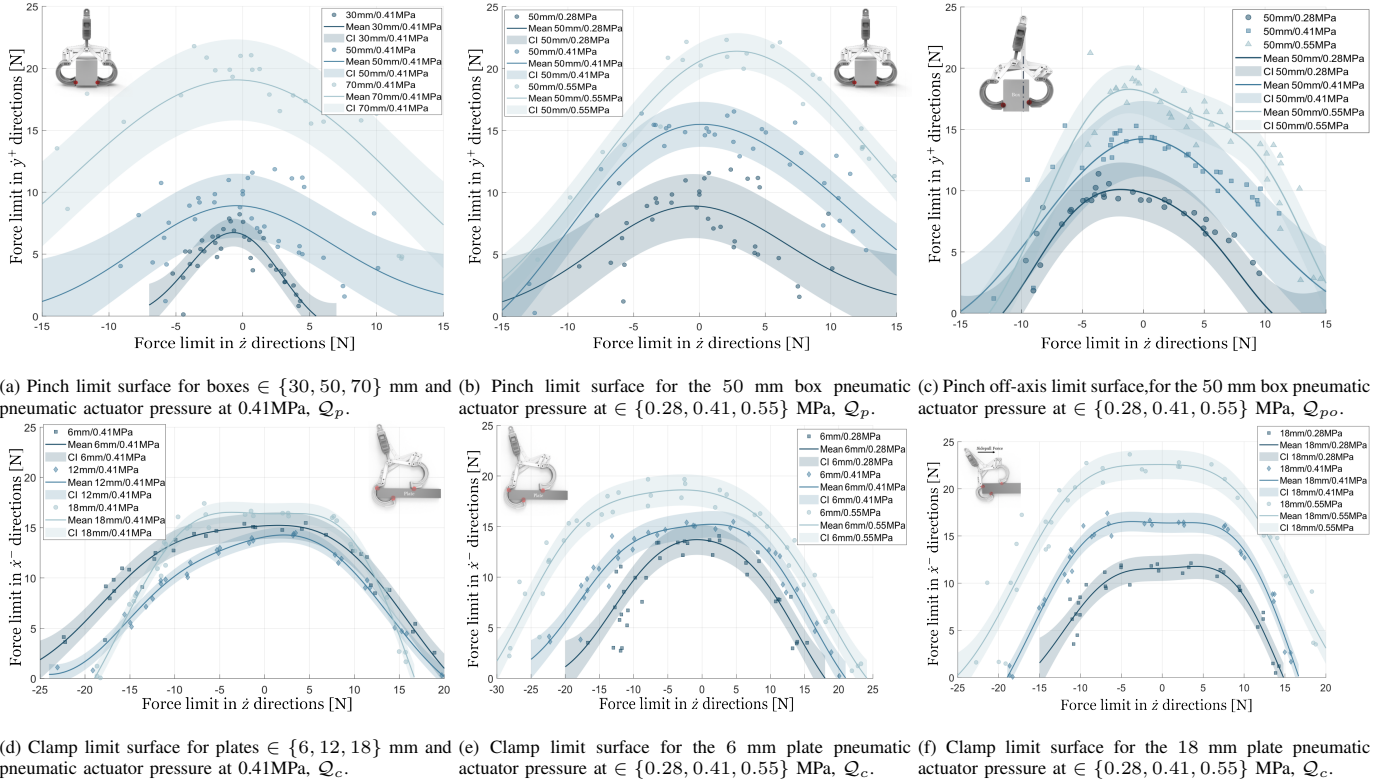


Fig. 18: Limit surfaces of the multi-modal C-GOAT gripper. For each data set, Gaussian Process Regression was applied to calculate the mean and confidential interval, CI. For pinch, \dot{y}^- direction will be symmetric. Data is collected without dry adhesive due to limited testbed manipulator arm force. The definition of $\eta \in \dot{x}, \dot{y}, \dot{z}$ in Table. IV.

TABLE V: Envelope mode mean pulling force in the \dot{y}^+ and \dot{z} directions. Values are mean of 3 and 6 trial for \dot{y}^+ and \dot{z} , respectively.

Pressure Diameter	Force limit in the \dot{y}^+ direction			Force limit in the \dot{z} direction		
	0.28 MPa	0.41 MPa	0.55 MPa	0.28 MPa	0.41 MPa	0.55 MPa
50 mm	73.0 N	102.7 N	116.3 N	7.6 N	13.0 N	18.0 N
60 mm	68.4 N	92.4 N	118.6 N	8.5 N	13.2 N	17.2 N
80 mm	43.1 N	54.7 N	67.7 N	10.5 N	17.5 N	22.9 N

TABLE VI: The mean maximum pulling force in the \dot{y}^+ direction for C-GOAT gripper pinch grasp on 50 mm box with and with no dry adhesive.

Pressure	0.28MPa	0.41 MPa	0.55 MPa
With dry adhesive \dot{y}^+ direction	36.4 N	54.5 N	78.4 N
With no dry adhesive \dot{y}^+ direction	8.9 N	15.5 N	21.4 N

E. C-GOAT Limit Surface Analysis

Here, we discuss the contact dynamics of seven grasping modes with the C-GOAT gripper. The spine-enhanced GOAT gripper's analysis is in [45]. All modes have distinct contact characteristics, resulting in unique constraints and limit surfaces as listed in Table. IV and corresponding limit surfaces in Fig. 18. The limit surfaces indicate the maximum force that each grasping mode can withstand in certain directions.

1) *Kinematic and Force Constraints*: Here we analyze the C-GOAT seven grasping modes kinematic and force constraints. For all grasping modes except hook, the \dot{z} directional velocities, \dot{z} in Table. IV, Fig. 17 are constrained to 0 if the force vector is in the respective limit surface. For the hook, the gripper cannot apply any normal force, and hence, there is no

bound for \dot{x}^- , \dot{z}^+ and \dot{z}^- . For the envelope grasp, the motion in \dot{y}^+ direction requires backdriving the gripper actuator to detach the gripper. The sidepull mode has physical constraints in \dot{x}^+ if the sidepull force condition is satisfied, as in Section IV-D2. If this condition is unmet, the grasp collapses to a pinch, oriented 90° around the z -axis.

2) *Grasping Mode and Limit Surface*: We collected the C-GOAT limit surface data Fig. 18 using the SCALER manipulator configuration shown in Fig. 9, equipped with the F/T sensor. The mean and 95 % confidence interval are calculated using Gaussian Process Regression (GPR) with a square exponential kernel. The tests were conducted without dry adhesive due to the arm's pulling force limitations. We have run separate experiments to determine the effectiveness of the dry adhesive. With dry adhesive in Table. VI, the maximum pulling force in the \dot{y}^+ direction is on average 3.7 times greater compared to the same grasp and object scenario in Fig. 18b, demonstrating a significant increase.

We analyze the limit surface of the pinch, off-axis pinch, clamp, sidepull, and envelope grasps to understand their contact force limit in the directions not physically constrained in the Table. IV. The limit surfaces are affected by the mode

of grasping, the object geometries, and the actuator forces as shown in Fig. 18 and Table. V. This contact analysis will be useful in the future for a grasping planner, etc. The pocket limit surface is equivalent to the pinch or pinch off-axis but with more kinematic constraints. The hook solely relies on finger geometries.

Pinch Grasp Analysis: First, we compare the pinch grasping on different object sizes and actuator force. The pinch grasp Fig. 18a force limit decreases for smaller objects due to the nonlinear force transmission of the GOAT mechanism [45], and the gripper kinematics significantly changes with this width range. The higher actuator force, such as higher gas pressures in Fig. 18b, increases the limit surface as the normal force at the contact rises. The off-axis pinch Fig. 18c exhibits a slight (< 2.5 N) skewness in the peak and asymmetry compared to the pinch in Fig. 18b. This is because the fingertip's normal forces are unequal due to off-axis grasping.

Clamp and Sidepull Grasp Analysis: The clamp grasp, on the other hand, shows consistent limit surfaces across the different plate thicknesses, as seen in Fig. 18d. This is because the gripper kinematics does not significantly change over these geometries, unlike the pinch grasp. The 18 mm plate is sidepull due to its thickness, and the 12 mm plate is close to the clamp thickness upper limit. Increasing the actuator force also expands the limit surface for clamp and sidepull in Fig. 18e, 18f due to increasing in normal force.

Pinch and Clamp Grasp Analysis: The \hat{z} directional limit (x -axis in Fig. 18) is higher for the clamp than for the pinch grasp. The clamp is a more constrained grasp, as in Table. IV with extra contact point. As discussed in Section IV-D, the sidepull can collapse to the pinch grasp. The sidepull has a larger limit surface in all directions in Fig. 18f even though the object is smaller (18 mm) compared to the pinch 30 mm in Fig. 18a.

Envelope Grasp Analysis: The envelope grasps in Table. V were tested for the cylinder diameters $\in \{50, 60, 80\}$ mm, which is close to the lower and upper bound of envelope graspable size. In the \hat{y}^+ direction force, the envelope grasp requires significantly higher forces than other limits in Fig. 18 since this backdrives the gripper actuator to detach the gripper as seen in Fig. 17c. As the diameter increases, this force limit decreases since less backdriving is required. Whereas, the results in the \hat{z} direction are consistent with those of the pinch grasp, as shown in Fig. 18, because both grasps share similar kinematic configurations. Hence, the limit force decreases as the object diameter decreases for the same reason as the pinch. The increase in the actuation force also increases limits in both directions across all sizes tested.

F. Grasping Force Controllers

The grasping force, or the normal force at each fingertip, is crucial in stable climbing. Increasing grasping force can help stabilize the grasp during incipient slipping [44], [55]. However, consistent grasping can generate excessive heat, degrading the DC actuator over time; hence, grasping force control is necessary. The DC linear actuated GOAT gripper includes the three controllers: 1) position control, 2) current-based force control, and 3) stiffness model-based force control.

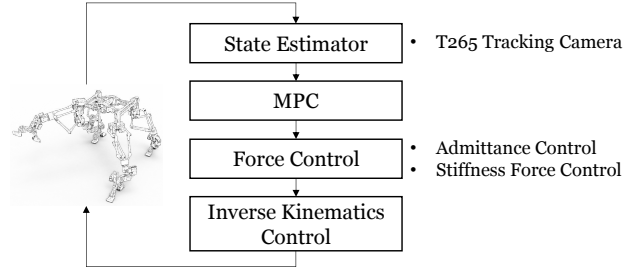


Fig. 19: SCALER software flowchart.

The pneumatic actuator only has an on-off control, which lacks any finger force feedback. However, it does not have an overheating issue, allowing it always to use the highest force output. More discussion on the tactile sensing limitation is in Section VII-B3. The MightyZap DC linear actuator by IR Robot features position and current-based force controls. The fingertip position is controlled with this position feedback and the gripper inverse kinematics. Stiffness model data is collected using a load cell while grasping different object sizes in [54]. The spine GOAT gripper maximum withstanding force has been modeled using Gaussian process regression in [45]. The model is stochastic due to the spine tip [53].

V. SCALER SOFTWARE

This section discusses SCALER's software, sensors, and control frameworks in Fig. 19.

A. Sensor-Actuator Interface and Frequencies

SCALER is equipped with various sensors: four F/T sensors on the wrists, a localization camera, a body IMU sensor, Dynamixel actuator encoders, and sensors on the GOAT gripper. The system's sensors and actuators operate at their respective maximum frequencies, which are sufficiently higher than the frequencies of controller modules. The Bota Rokubi F/T sensors operate at 800 Hz, the Intel RealSense T265 localization camera is set to 200 Hz, and the Microstrain 3DM-GX4-25 IMU runs at 500 Hz. Meanwhile, the Dynamixel communicates at 400 Hz via RS-485 and a USB serial bus. Each limb features a redundant communication chain for robustness and safety. The wrist and gripper actuators are connected to the shoulder power and communication distribution board via a M12 cable.

B. State Estimation

SCALER employs the vision SLAM T265 camera to track the current trunk state with respect to the world reference frame. Kinematics and joint encoders are used to determine all four end-effector states. The T265 camera tracking is analyzed using SCALER walking configuration in [56]. For bouldering wall holds, [12] demonstrated primitive-based sparse object mapping, which estimates the hold's pose and shape as an ellipsoid. The reported hold pose and shape estimation errors are ± 4 mm and 12 % of their size [12]. In this paper's experiments, we have not utilized this mapping framework due to limitations such as cases where the limbs are in view and disturbing the depth images.

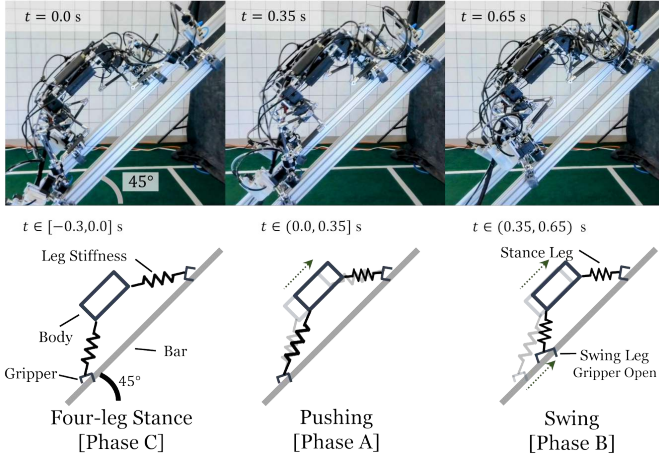


Fig. 20: SCALER modified trot gait on the 45° slope. SCALER starts from the end of **Phase C**. For **Phase A** $t \in (0.0, 0.35]$ s SCALER push the ground and stiffen the leg to increase the support force on the stance leg. For **Phase B** $t \in (0.35, 0.65]$ s, two diagonal RB/LF legs pair here swings to the next footsteps. For **Phase C** $t \in (0.65, 0.95]$ s SCALER closes grippers and is in 4 leg stance. The kinematic drawing illustrates the two legs and the body motions with imaginary linear leg springs for visualization purposes.

C. Force Admittance Control Framework

Admittance control is employed to track desired operational space force profiles in contact-rich tasks. Wrench or force tracking is essential to sustain dynamic stability and mitigate disturbance due to premature or unintended contacts. The control framework (4) extends the formulation in [57] to accommodate the wrench reference trajectories. Each leg has an independent admittance controller.

$$K_f(\mathbf{W} - \mathbf{W}_{\text{ref}}) = M_d \ddot{\mathbf{x}} + D_d \dot{\mathbf{x}} + K_d(\mathbf{x} - \mathbf{x}_{\text{ref}}) \quad (4)$$

Here, K_f , M_d , D_d and K_d are the user-defined diagonal admittance control gain in \mathbb{R}^6 , \mathbf{x} , $\dot{\mathbf{x}}$ and $\ddot{\mathbf{x}}$ are the end effector 3D pose and its first and second derivative. \mathbf{W} is a 3D wrench vector. \mathbf{W}_{ref} and \mathbf{x}_{ref} are the desired wrench and pose. The control input is the double integral of $\ddot{\mathbf{x}}$. The \mathbf{W} is estimated with the F/T sensors and the method described in [54]. The \mathbf{x} and $\dot{\mathbf{x}}$ are measurements.

Due to gear backlash, the controller struggles to track rapidly changing force profiles [54]. This control bandwidth suffices for low-speed tasks such as quasi-static climbing that experience less frequent force reference changes. The admittance controller experiments are shown in [44] and [54].

D. Model Predictive Control

Model Predictive Controller (MPC) disturbance rejection becomes more important when SCALER conducts dynamic motion with the pneumatic actuators since the gripper induces disruption. Our MPC employs linearized discrete-time dynamics based on a single rigid body model affected by ground reaction forces at the patch contacts in (5), which is adapted from [58]. A_k and B_k are the discrete-time linearized dynamics models at a discrete time, k , and shown in equations (6) and (7), $\mathbf{x}_k^{\text{mpc}} \in \mathbb{R}^{12}$ is the trunk state, where the first three components include roll, pitch, yaw, the next three the position, and the rest the angular and linear velocity respectively, \mathbf{x}_k^n is

the 3D pose of the end-effector for limb n in the body frame, $\mathbf{f}_k^{\text{mpc}}$ is a ground reaction force, $\hat{\mathbf{I}}$ is the inertia tensor matrix in world coordinates m is the total mass of the robot's body, $[\bullet]_{\times}$ is defined as the skew-symmetric matrix, and $\mathbf{I}_3 \in \mathbb{R}^{3 \times 3}$ is an identity matrix, $O_{u \times w} \in \mathbb{R}^{u \times w}$ is a zero matrix.

$$\mathbf{x}_{k+1}^{\text{mpc}} = A_k \mathbf{x}_k^{\text{mpc}} + B_k \mathbf{f}_k^{\text{mpc}} + \mathbf{G} \quad (5)$$

$$A_k = \begin{bmatrix} O_{3 \times 6} & \mathbf{R}_{b,k}^{w\top} & O_{3 \times 3} \\ O_{3 \times 6} & O_{3 \times 3} & \mathbf{I}_3 \\ O_{6 \times 6} & O_{6 \times 3} & O_{6 \times 3} \end{bmatrix} \quad (6)$$

$$B_k = \begin{bmatrix} O_{6 \times 3} & \dots & O_{6 \times 3} \\ \hat{\mathbf{I}}^{-1} [\mathbf{x}_k^1]_{\times} & \dots & \hat{\mathbf{I}}^{-1} [\mathbf{x}_k^n]_{\times} \\ \mathbf{I}_3/m & \dots & \mathbf{I}_3/m \end{bmatrix} \quad (7)$$

The gravity vector, \mathbf{G} in (8) changes based on the climbing environment, such as a slope, vertical, or ceiling, though \mathbf{G} is still a constant given a known slope. R^{Wall} is the wall rotation matrix in $SO(3)$ with respect to the Earth's local tangent plane frame, and $g \in \mathbb{R}^1$ is a gravitational acceleration constant.

$$\mathbf{G} = \begin{bmatrix} O_{9 \times 9} & O_{9 \times 3} \\ O_{3 \times 9} & R^{\text{Wall}} \end{bmatrix} \begin{bmatrix} O_{11 \times 1} \\ g \end{bmatrix} \quad (8)$$

Since SCALER has high-gear ratio servos, we do not directly convert the control outputs from our MPC, or $\mathbf{f}_k^{\text{mpc}}$ into joint torques, as done in [58], but instead use them as a reference to lower level position based force controllers such as our admittance controller, as demonstrated in [54]. In our experiments, positions are commanded. Note that we only used this closed-loop MPC for the untethered experiments with the modified trot gait. The lower control bandwidth of the admittance controller bounds the MPC performance. The MPC runs at 100 Hz, and the state estimators run sufficiently faster.

VI. HARDWARE EXPERIMENT

In this section, the performance of SCALER in various climbing and ground locomotion tasks is evaluated to address the following questions:

- 1) SCALER's capabilities for dynamic locomotion on the ground and dynamic climbing on the slope.
- 2) Its power-intense motion capacities, e.g., payload, in each of these scenarios.
- 3) Performance in inverted environments (e.g., ceiling), including slippery terrains.
- 4) Multi-modal and whole-body grasping in free-climbing.

During these experiments, an off-board computer and external power supply were used to operate SCALER as precautionary measures. The fully untethered operation is covered in Section VI-A5. The energy consumption stochastically fractures from 50 W to 220 W for climbing. The highly constrained scenario, such as SCALER grasping environments, can cause internal forces, which temporarily increase power consumption. All reference trajectories in the experiments were predefined manually. The details on fully autonomous contact-rich free climbing planning are in [44].

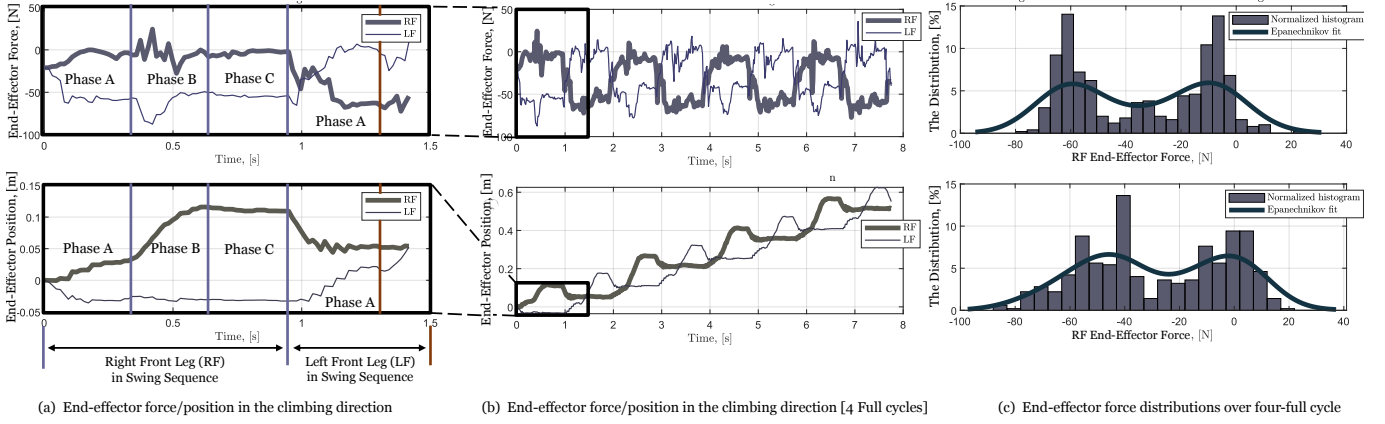


Fig. 21: Foot force and position graphs over time, and force distribution over four full cycles of the modified trot gait. SCALER end effector climbing direction force and estimated foot position were recorded at 64.3 Hz in Section VI-A2. SCALER swings LF first and then RF. The first sequence was half stride lengths compared to the rest. (a) End-effector force and position of RF and LF for the firstb sequence in Fig. 20. (b) The four-full gait cycle end-effector force and position. (c) Histogram of the RF and LF force over the four-full gait cycle with Epanechnikov kernel smoothed curve fitting.

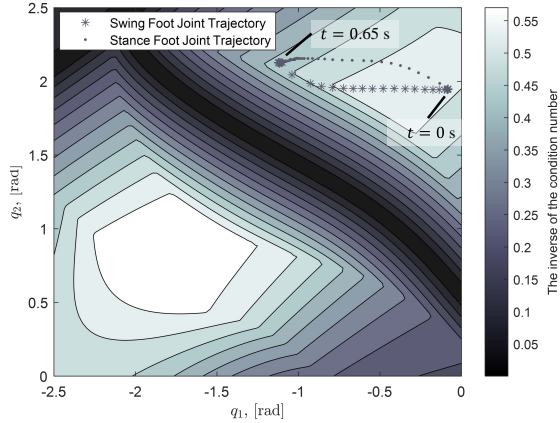


Fig. 22: SCALER leg stiffness map. The inverse of the stiffness condition number at $q_0 = 0$ rad, where $q_i, i \in \{0, 1, 2\}$ are the shoulder, back, and front linkage motor joints in Fig. 7. The joint trajectory is from RF in the modified trot gait in Section VI-A2. The RF leg is in stance sequence, and the corresponding configuration is at $t = 0.0$ s and $t = 0.65$ s in Fig. 20.

A. Dynamic Locomotion

1) *Trot Gait on the Ground*: First, we evaluate SCALER's dynamic locomotion capability on the ground. SCALER trotted at 0.56 m/s, or normalized body velocity of 1.87 s^{-1} , normalized based on the body length. This trot velocity was recorded based on the video frame. SCALER 3-DoF walking configuration demonstrated that SCALER can trot at a comparable normalized velocity to recent ground quadruped robots as in Table VII.

2) *Dynamic Climbing with Modified Trot Gait*: In this experiment, we demonstrate SCALER's dynamic climbing capability using the proposed modified trot gait on the hardware. Dynamic climbing introduces a new set of challenges for SCALER, as mentioned in Section III-D2. SCALER equipped with C-GOAT grippers performed the modified trot gait on the 45° sloped aluminum bars, as seen in Fig. 20. This terrain is slippery and has low friction.

SCALER reached 0.077 m/s or a normalized velocity of 0.27 s^{-1} . This was 13.8 times faster than demonstrated in

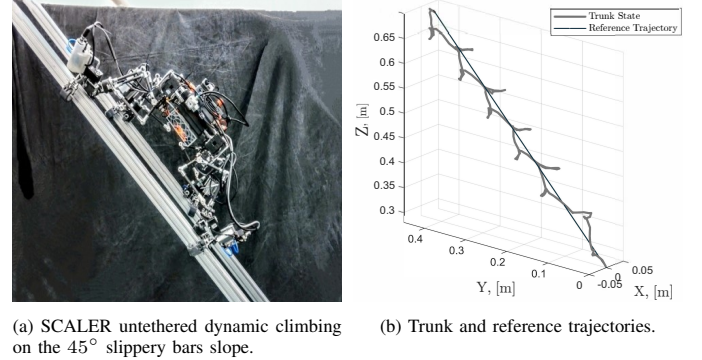


Fig. 23: SCALER untethered modified trot gait.

[12]. We observed consistent climbing overall for this environment, which was successful for 36 consecutive steps over three separate runs. We observed no failure cases for this environment, though the dry adhesive showed wear over time. The fastest climbing with a DC-actuated GOAT gripper is in Section VI-D3, during which the robot was idle for 57.3 % of the time because the gripper takes 8.6-second for the opening and closing cycle. This bottleneck is overcome by the C-GOAT grippers, which take 0.2 s for the cycle.

3) *Efficacy in Sag-Down Mitigation with Modified Trot Gait*: This section validates the modified trot gait's effectiveness in reducing sag-down during dynamic climbing. Climbing direction end effector force and position were measured using F/T sensors and the T265 camera. The gait sequence details are in Section III-D2, and each phase is visualized in Fig. 20.

In Fig. 21a shows forces and positions in the climbing direction (i.e., the direction of the aluminum bars) for the first 4 phases, and Fig. 21b is data for 4-full cycles of the gait. Fig. 21c is the normalized force histogram over the 4-full gait cycle. At $t = 0$, the RF leg is in the swing sequence.

In **Phase A**, the RF force drops to nearly zero, while that of the LF's doubles due to the pushing action, indicating successful support force and leg transition. This causes a slight position 'drop,' which is interpreted as an 'imaginary slip.' The T265 camera estimator assumes rigid legs where the actual

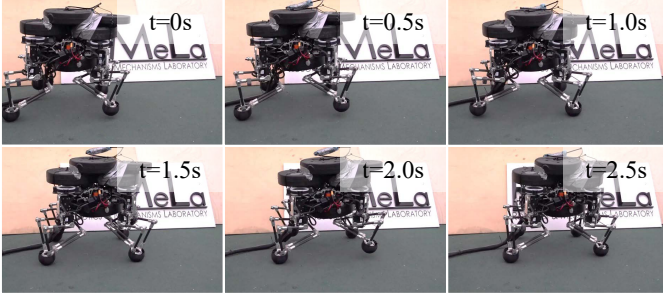


Fig. 24: SCALER 3-DoF leg walking configuration with a 14.7 kg payload, equivalent to 233 % of its weight.

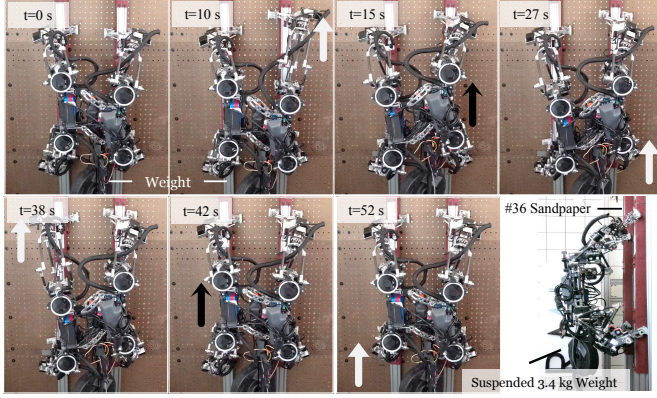
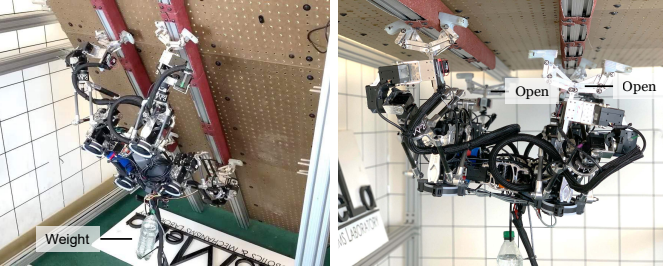


Fig. 25: SCALER climbs a vertical wall with a 3.4 kg payload using the SKATE gait. White and black arrows indicate leg swing and body motion, respectively. The gait schedule is illustrated in Fig. 12a. Phase 0 at 10 s, followed by Phase 1 at 15 s and Phase 2 at 27 s, while the left side of the legs remains stationary. Then, the LF enters Phase 0. The SKATE gait sequence took 52 s to travel 0.14 m, achieving a speed of 0.16 m/min.



(a) Climbing on an overhang wall at 125° . (b) Two finger support on the ceiling.

Fig. 26: SCALER under inverted environments. A weight hangs from the robot to indicate the direction of gravity.

limb has compliance, which detects the apparent but non-actual slip. **Phase B** sees RF gripper force disturbances as it swings forward. **Phase C** closes grippers and maintains a 4-leg stance for stability.

The distinct force/position pattern repeats over four trot gait cycles. The two peaks in Fig. 21c represent the forces during stance and swing sequences. Skewness in these peaks between RF and LF suggests the robot is tilting toward RF.

In summary, the modified trot gait has achieved the intended gait design objectives, confirmed by both experimental data and an attached video showcasing SCALER's successful climb, compared with a failed conventional trot gait case.

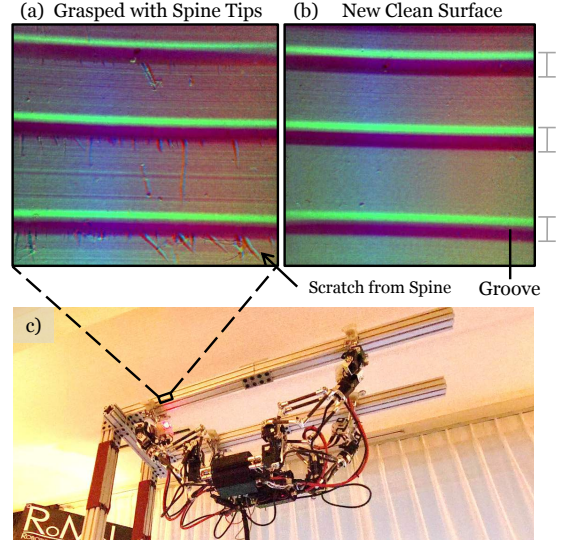


Fig. 27: Tactile images capturing the surface of the T-slotted aluminum bar and its interaction with SCALER's spine tips. (a) The tactile image shows scratches from spines compared to the new aluminum bar shown in (b). (c) SCALER with spine tip GOAT grippers can travel upside down on a slippery surface due to this spine effect.

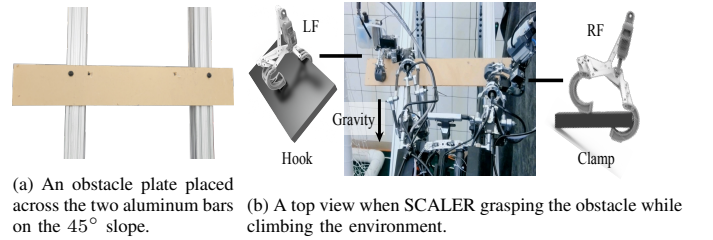


Fig. 28: The environment and the top view for SCALER climbing using three modes of grasping: pinch, hook, and clamp to overcome a thin plate obstacle.

4) *Limb Stiffness Model and Force Analysis:* The VJM model in Section III-B2 is calculated, and the stiffness map is in Fig. 22, which is the inverse of the stiffness condition number. The valley in the stiffness map visualizes the stiffest regions [59]. The joint trajectory recorded from the experiment in Section VI-A2 is plotted on the stiffness map in Fig. 22. This indicates that the leg stiffens when pushing in the modified trot gait. The stiffness of each joint was measured using a Mitutoyo HD-12 AX, which applied a force on the F/T sensors to deform the joint.

The pushing force during **Phase A** in Section VI-A2 is estimated to be 31.7 N using VJM given the commanded 0.16 m pushing distance in the climbing direction. The pushing force generated from the LF in **Phase A** in Fig. 21a is 37.3 N on average. Our stiffness model provides adequate stiffness estimation for the SCALER's climbing tasks, with an average of 17.6 % modeling error for this modified trot gait case.

5) *Untethered Climbing using C-GOAT with MPC:* SCALER can operate fully untethered when equipped with the computing and power modules. This represents SCALER's ability to go off-grid and climb with no range limit due to the tethering. Fig. 23a shows the SCALER climbing on a 45° slippery slope untethered with MPC presented in Section V-D, and Fig. 23b is the trunk states from the T265 camera. The

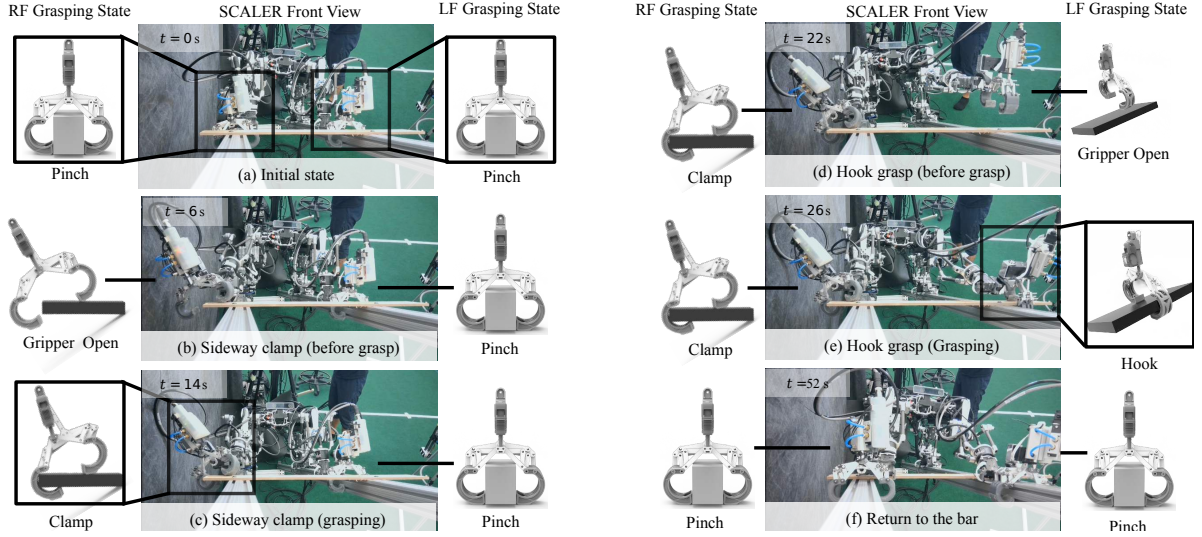


Fig. 29: Front views of SCALER climbing the environment with an obstacle thin plate in the way shown in Fig. 28. SCALER utilized pinch, clamp, and hook grasp modes to overcome the obstacle so that it can continue to climb. RF and LF grasping states render the SCALER’s gripper grasping modes. (a) SCALER grasping aluminum bars before entering the obstacle region. (b), (c) SCALER clamped the thin plate from the side. (d), (e) SCALER hook the gripper on the thin obstacle plate. (f) SCALER moved both front arms back to the bar. It took 60 s to reach the state (f) from (a).

experiment was repeated once. MPC showed improvement in the tracking in the x -axis in Fig. 23b particularly (open-loop 35 mm, MPC 1.6 mm offset after 12 steps).

B. Payload Capacity

1) *Ground Trot with Payload*: To benchmark SCALER’s load capacity compared to other quadruped robots, we attached a payload of a 3.4 kg weight to its belly and an 11.3 kg weight on the top, corresponding to 2.33 times its own weight. The trotting velocity of SCALER with the 14.7 kg payload was at 0.13 m/s, or a normalized velocity of 0.33 s^{-1} . This payload was the maximum SCALER can trot, but it struggled to move in a straight direction. A payload of 10.2 kg yielded a speed of 0.25 m/s, and SCALER was able to trot in a straight line. A normalized work capacity, defined as $WC = V \times P$, where V and P represent normalized maximum body velocity and payload, respectively, provides a quantitative metric for SCALER’s mechanical efficiency of legged robots [60]. SCALER outperformed other robots with the normalized workload capacity of 3.88 [60].

2) *Vertical Wall SKATE Gait Climbing with Payload*: In this experiment, we evaluated SCALER’s mobility in vertical climbing with a payload. We tested SCALER on a vertical wall outfitted with a straight 0.05 m wide rail covered by #36 sandpaper to simulate rock surfaces. Each gait sequence lifted the body by 0.075 m and achieved a speed of 0.16 m/min while carrying a 3.4 kg payload. This accounts for 35 % of SCALER’s total weight. Suspended payloads pose challenges due to pendulum dynamics. The black and white arrows in Fig. 25 indicate which leg and body motions compared to the previous frame, respectively. The same experiments were conducted twice for consistency. SCALER demonstrated vertical climbing with a payload, indicating the SCALER’s power-intensive motion and the GOAT gripper capabilities.

C. Inverted Environments

In inverted environments, such as overhangs and ceilings, the effectiveness of the grippers becomes pivotal. These grippers must exert sufficient contact force to counteract the gravitational pull.

1) *Overhang Climbing*: SCALER climbed on an overhanging wall tilted at 125° towards the robot in Fig. 26a. A weight of 0.5 kg was suspended from the robot’s body to indicate the direction of gravity. We conducted overhang and vertical climbing for this environment three times each. In this environment, gripper weight helped the spine fingertips to break the contact when lifting limbs. Although there was no failure, there was a case in vertical climbing where the back limb gripper’s finger stuck due to the spine, and the stride distance for this limb was shorter than the commanded stride.

2) *Upside-down Ceiling Walk On Rough Surfaces*: When SCALER operates in an upside-down orientation on the ceiling, SCALER uses spine fingertip GOAT grippers to grasp the rails on the ceiling in Fig. 1a. The 0.5 kg weight is suspended from SCALER. This experiment was repeated twice.

The effects of the fingertip spine enhance gripping as data presented in [45] for the GOAT gripper. These effects enable SCALER to maintain a stable grip on the ceiling, even when only two grippers are grasping, as shown in Fig. 26b. Furthermore, these finger spines allow SCALER to remain attached to the ceiling or a vertical wall even when the system is powered off. The spine effects can generate sufficient shear force with minimal normal force as long as the needle tips remain engaged with the surface microcavities.

3) *Upside-down Ceiling Walk on Slippery Metal Surface*: In this experiment, we evaluate the spine GOAT grippers on a slippery aluminum surface as pictured in Fig. 27a,b with Gelsight Mini tactile sensors [61]. SCALER successfully walked on a T-slotted aluminum bar upside down in Fig. 27c. The spines engaged with micro textures on the aluminum bar surface, generating enough shear force to support SCALER

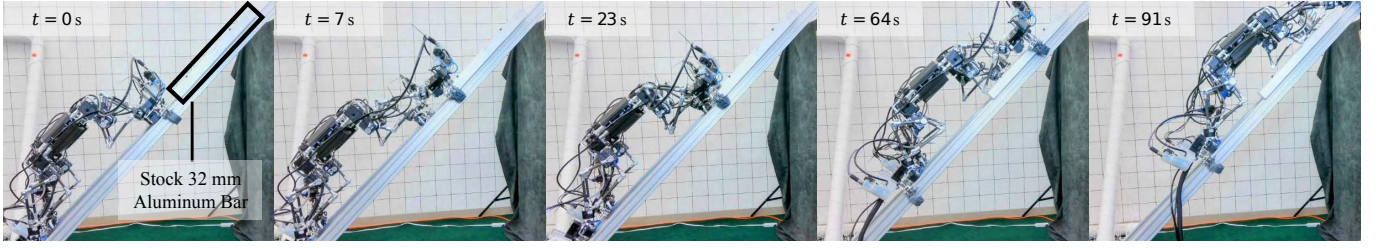


Fig. 30: The whole-body approach with side-pull techniques. The obstacle plate, marked in a black box, is too thick to clamp, but with the whole-body approach, SCALER can side-pull to stabilize itself. The force graph indicates a significant sideways force generated by SCALER in Fig. 32. SCALER started from the aluminum bars and conducted the sidepull whole-body climbing from $t = 7$ s. SCALER reached the top of the obstacle and returned to the bar at 91 s.

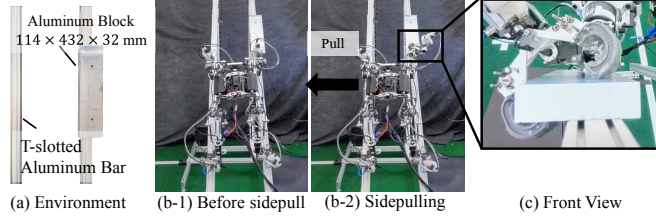


Fig. 31: SCALER climbing the aluminum bars with an obstacle plate in the way. (a) The test environment with a stock aluminum plate attached on one side of the bars. (b-1) A top view before sidepull. (b-2) when sidepulling. (c) A front view of the sidepulling GOAT gripper.

upside down on the slippery surface. The tactile images shown in Fig. 27a,b compare the aluminum bar surface grasped with the spine and a new unused identical aluminum bar. The spines caused scratches at the bottom edge of the grooves in Fig. 27a. These etches indicate that the spines are anchored in the grooves to generate shear forces, whereas spines making contact on the flat aluminum surfaces do not contribute to this shear force significantly. Since the environment is very slippery, there was no case when the gripper stuck like with sandpaper environments in Section VI-C1 over four episodes.

D. Multi-Modal and Discrete Terrains Free-Climbing

This section focuses on SCALER's loco-grasp free-climbing capabilities in directionally continuous (Fig. 2c) and discrete environments (Fig. 2b).

1) Climbing over Obstacles with Multi-Modal Grasping:

We experiment with SCALER's ability to overcome obstacles while climbing through multi-modal grasping. SCALER leverages the C-GOAT grippers to climb by grasping obstacles. A 6.5 mm plate obstacle was placed across the T-slotted aluminum bar oriented at 45° as shown in Fig. 28a. SCALER clamps and hooks the obstacle plate from the side and top to continue climbing as captured in Fig. 28b. This capability enhances the SCALER's traversability since it can utilize obstacles instead of avoiding them.

Fig. 29 shows the front view of SCALER conducting multi-modal grasping with rendering of the RF and LF grasping states. Fig. 29b,d pictures that SCALER orients and aligns the grippers to clamp and hook the plate. Obstacle traversing behavior is done with manual trajectory here. Out of 10 trials, clamp and hook were successful 9 and 4 times, respectively. The hook tended to fail because the back of the finger caused

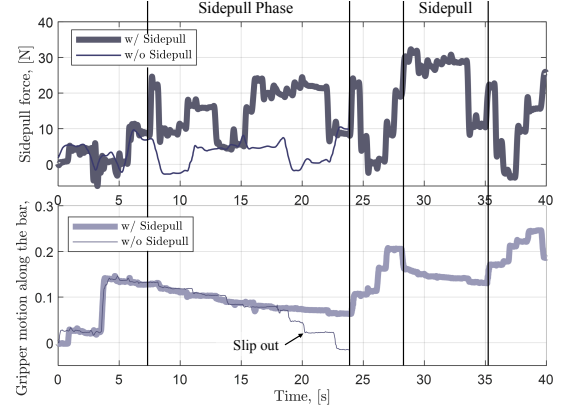


Fig. 32: Sidepull forces and sidepulling gripper motions in the climbing direction. Without sidepull, the gripper slid out, and SCALER could not continue climbing. With sidepull, SCALER climbed and back to the bar at 91 s in Fig. 30.

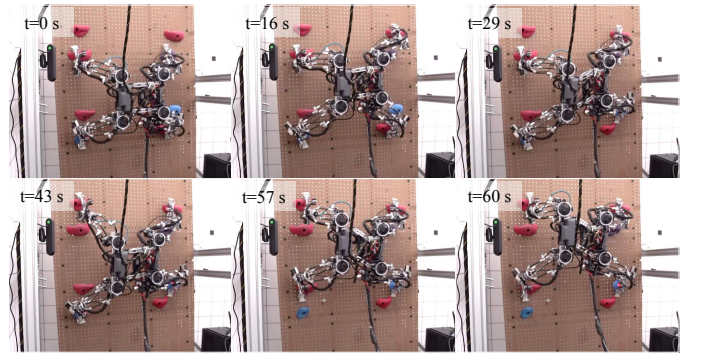


Fig. 33: SCALER climbs a bouldering wall after each leg moves forward. The wall is at 90° . SCALER climbed up 0.35 m at 0.35 m/min.

unexpected contact with the plate, and one episode was fully successful in one shot.

The success of the multi-modal grasping method signifies SCALER's dexterous capabilities, making it more versatile in traveling complex terrains than traditional climbing robots.

2) *Whole-body Approach in Climbing:* We explore SCALER's whole-body climbing strategy for overcoming difficult-to-grasp obstacles, as displayed in Fig. 30 and 31. Fig. 32 contrasts the RF gripper's sidepull forces and positions in the climbing direction with and without sidepulling. The whole-body approach integrates the capabilities of both GOAT grippers and SCALER.

When confronted with a thick, slippery obstacle plate, as

TABLE VII: Performance of quadruped robots on the ground comparisons. [60].

Robot	DoF per Limb	Weight (kg)	Normalized Payload (Unitless)	Max Payload (kg)	Normalized Speed (s^{-1})	Ground Velocity (m/s)	Normalized Workload (Unitless)
SCALER (Walking)	3	6.3	2.33	14.7	1.87	0.56	3.88
ANYmal	3	30	0.33	10	1.0	0.8	0.33
Stanford Doggo [21]	2	4.8	N/A	N/A	2.14	0.9	3.2
Titan XIII	3	5.7	0.89	5	4.29	0.9	3.79
SPOT	3	30	0.47	14	1.45	1.6	0.68
Mini Cheetah	3	9	*1	*9	6.62	2.45	N/A

Normalized Velocity: body length divided by the body velocity. Normalized Payload: body weight divided by payload. Normalized Work Capacity: normalized speed \times normalized payload, a mechanical efficiency metric [60]. *The value is theoretical.

TABLE VIII: Performance of multi-legged robots for climbing comparisons.

Robot	DoF per Leg / Gripper (Passive DoF)	Climbing Gravity	Climbing Velocity m/min	Normalized Velocity m^{-1}	Climbing Payload kg	Gripper	Environment
SCALER	6/1	Earth, g	4.62	13.2	3.4	Two finger Spine, Dry adhesive GOAT Gripper	Discrete Fig. 2b, Overhang Fig. 2c, Ceiling Fig. 2c Slippery surface
LEMUR 3 [18]	7/2	Mars, Moon, Zero 0.38, 0.17, 0 g	$2.7e^{-3}$	$6.7e^{-3}$	N/A	Radial Velcro-like Spine Gripper	Continuous Fig. 2a Rough
HubRobo [1]	3(3)/1	Mars 0.38 g	0.17	0.57	N/A	Radial Passive Spine Gripper	Discrete Fig. 2b
Slalom [16]	4(3)/0	Slope: $30^\circ \sim 0.5 g$	6	17.1	N/A	Dry Adhesive EPDM Rubber	Flat Solid/Soft Fig. 2a
RiSE [24]	2/0	Earth, g	15.0	40.0	1.5	Spine Array	Continuous Fig. 2a Rough
Bobcat [22]	2/0	Earth, g on strap	10.5	22.8	N/A	Spine Array	Continuous Fig. 2a Wire Mesh
Climbot [6]	2/1	Earth, g	2.2	N/A	N/A	two-fingered Gripper	Pipe Fig. 2c
MARVEL [17]	3(3)/0	Earth, g	42.0	127.2	2	Electropermanent Magnetic	Continuous Fig. 2a Ferromagnetic w/ Paint

Climbing Gravity: simulated gravity used in their robot climbing tests, where $g \in \mathbb{R}^1$ is a gravitational constant. Climbing velocity: the robot's body velocity while climbing. Normalized velocity is the climbing velocity normalized by the robot's body length. * The body length of LEMUR 3 is approximated as the half track length in [18]. EPDM stands for Ethylene Propylene Diene Monomer.

depicted in Fig. 31a, SCALER employed a sidepull technique. The plate's dimensions made it not possible to employ a pinch or a clamp grasp in a stable manner, necessitating the whole-body sidepull approach. Fig. 31b-1 and 31b-2 visualize SCALER pushing itself to the left and employing a sidepull using the RF GOAT gripper. The close-up gripper front view in Fig. 31c resembles the sidepull rendered in Fig. 17f. Successively, 64 steps were conducted for this case over two experiments.

In the sidepull phase displayed in Fig. 32, SCALER applied lateral force to the RF gripper using a creep gait (Fig. 12b), enabling stable grasping. The minimum required sidepull force was estimated at 15.8 N based on (3). The cases, with and without sidepull, slipped at a similar rate until $t = 16$ seconds because the sidepull force was insufficient. The case without sidepull couldn't meet this force requirement and slipped completely by $t = 20$ seconds. The case with sidepull stabilized after reaching 20 N. This indicates that the sidepull force can stabilize the grasp, and the sidepull force calculation aligns with the results. SCALER successfully traveled over the 432 mm obstacles and returned to the aluminum bar. The mean supporting force, the magnitude of the forces normal and parallel to the bar, is 72% higher than the failure case. Hence, the sidepulling with the proposed C-GOAT gripper was relied on by SCALER for this whole-body approach.

This whole-body strategy enhances SCALER's traversability further and demonstrates the symbiotic potential between

the robot and its gripper in climbing.

3) *Bouldering Vertical Free-Climbing*: This experiment demonstrates SCALER's ability to climb in discrete environments, particularly on a vertical bouldering wall. GOAT grippers have to grasp bouldering holds with a non-convex shape. Conventional polymer-made bouldering holds were installed on a 90° wall, and SCALER was operated using a predefined manual trajectory. SCALER successfully climbed up for four steps in Fig. 33, and each leg moved to the next bouldering hold at 0.35 m/min or a normalized speed of 1.0 min^{-1} . Over five trials, 12 out of 16 steps were successful, and one episode was fully successful with an open-loop trajectory. SCALER stretched the legs farther with the torso mechanism such as at $t = 29s$ and $t = 57s$ in Fig. 33, representing the kinematics benefit of SCALER's torso DoF.

SCALER's performance in the bouldering wall environment illustrates its potential in applications where maneuvering in discrete, unstructured environments is necessary. More discrete environment climbing with obstacles was tested in [44].

VII. DISCUSSION AND LIMITATION

In this section, we discuss key takeaways and limitations from our experiments. Results from hardware experiments are compiled and summarized in Table. VII, VIII. Table. VII contrasts the SCALER 3-DoF walking configuration with other legged robots such as ANYmal and SPOT, revealing that SCALER achieves comparable normalized speeds. Notably,

SCALER surpasses all other quadrupeds in its ability to carry a payload over twice its weight and normalized work capacity, as evidenced in [60].

Table VIII compares SCALER to other state-of-the-art climbing robots to SCALER regarding their operation environments, end-effector, and capabilities. SCALER has successfully shown traversability in various directions of gravity and versatile climbing performances across different climbing holds. We can distinguish climbing robots based on whether they have multi-finger grippers or not. This is a notable difference since the adhesive type of end-effectors can reduce the climbing problem down to locomotion under different gravitational force directions. Suction [32], magnetic [17], and gecko or Van der Waals force-based end-effectors generate normal forces regardless of the direction of gravity. Therefore, if such an end-effector can provide enough adhesive forces, the robot does not need to consider dexterity or grasping explicitly.

A. Limitation

1) *Rigidity and Compliance*: Since SCALER is a loco-grasping platform, balancing conflicting requirements presents a design challenge. Rigidity in joints and linkages provides the benefit of accuracy and repeatability in position-controlled manipulation under load [62], while compliance offers mechanical adaptability [39]. Such adaptability is useful for compensating for system and environment uncertainties.

Nonetheless, we observed failure cases in experiments due to leg compliance in high-friction environments such as sandpaper in Section VI-C1 and in [44]. When SCALER approaches an object with a high-friction surface, it can fail to grasp the object if one of its fingers makes an undesired contact. In position control settings, the leg stiffness limits the force required to break this undesired contact unless the joint reaches its torque limit. This limitation arises because the deflection is solely due to the difference between the intended goal position and the point where the undesired contact occurs.

SCALER leg consists of three major compliance sources: parallel link mechanisms, gear backlash, and wear. The passive joints and carbon fiber tubes are relatively compliant, though the SCALER's two redundant front linkages enhance rigidity. The SCALER's actuators use spur gear with 0.25° backlash, translating to the maximum 1.65 mm offset given leg length. Over time, the gear and output shaft wear increase backlash and the task-space position control inaccuracy. The model in Section III-B2 helps us understand the characteristics of the SCALER leg compliance and we utilized it for stiffness force control. Leg compliance has been accounted for in planning as demonstrated in [34] and [37].

2) *Limb Dexterity*: Another metric for evaluating grasping capability is the dexterous workspace. While dexterity can be improved by eliminating the end-effector offset from the spherical wrist, practical considerations such as gripper geometries and potential collisions with environments must also be accounted for. Although the variants of the SCALER wrist in Fig. 8 have sufficient joint range for our designated tasks, the workspace can be constrained by self or environmental collisions, depending on the gripper's orientation and the

position of the parallel link elbow joint. Consequently, it is important to consider potential collisions when planning trajectories along with kinematic and dynamic feasibility for all legs, fingers, and the body to ensure safe climbing.

3) *Uncertainty and repeatability*: In order to conduct safer and more robust climbing, it is essential to consider the uncertainty in the system [37]. Stochasticity in the grasping contacts, particularly with the spine, introduces large variance in the maximum force it can sustain [37], [45]. For discrete environments, repeatability is subject to the initial robot state since our trajectory is generated offline, and the estimator tracks the state with respect to the initial state. From Section VI-D1 and VI-D2, the hook success rate was 40 %, which is less than pinch, clamp, and sidepull. The hook grasp required more positional accuracy since it relied on the kinematical constraints, as shown in Table. IV.

Localization and state estimation errors are more critical in discrete environments. GOAT gripper's adaptiveness provides margins, but the estimation error can accumulate over time [56]. In future work, additional mechanisms, such as visual servo, will be necessary to compensate for the accumulated error, leading to a higher success rate of tasks.

B. GOAT Gripper Limitation

1) *Contact State Transitions*: The GOAT gripper features spine-enhanced fingers that aid in grasping by penetrating an object's surface cavities. While the spine has shown notable performance in our experiments, the spine-enhanced fingers can also act as a barrier to gripper state transition due to their strong adherence. When the spine fingertip contact breaks during the opening and lifting of the gripper, the internally stored energy in leg compliance is released abruptly, which can cause a non-negligible disturbance to the robot. This potentially accelerates the wear and damages the spine tips, reducing the life cycle of the finger, which is a common issue in spine grippers [18].

2) *Macro and Micro Scale Contacts*: Although the C-GOAT gripper can realize various grasping types, it can only explicitly consider larger-scale contact modes. However, relatively small-scale surface feature and dynamics significantly affects the success of grasping [63]. In Fig. 27c, SCALER can walk upside-down with spine tips on metal bars. However, spine tips require a covered surface for vertical climbing, and SCALER could not climb vertically on the bare aluminum bar. The T-slotted aluminum has grooves along the bar, as shown in Fig. 27b. In the vertical case, spines only resist force perpendicular to the grooves but not gravitational force in the direction of the bar and grooves. Hence, SCALER slips down along the grooves because pure friction force between the spine tips and the aluminum surface is insufficient. Hence, small-scale texture variations have significance, and improving micro contact properties, such as demonstrated in [64], can potentially benefit climbing robot graspability.

3) *C-GOAT C-Shaped Finger Contacts*: The C-GOAT gripper enables SCALER to achieve multiple modes of grasping in climbing. However, the C-shaped finger has limited contact areas due to its curvature. Consequently, this design requires

a significantly larger normal force, as the dry adhesive contact depends on the real molecular-level contact area [64]. The pneumatic actuator used with the C-shaped finger in the GOAT gripper generates twice the normal force compared to the DC linear actuator. Furthermore, the state estimation of all seven modes remains an open problem.

VIII. CONCLUSION

The SCALER mechanisms, including torso and limb designs, coupled with the GOAT gripper, constitute a versatile loco-grasping platform capable of traversing various challenging terrains. SCALER's parallel-serial hybrid limb designs have adequately accomplished body dynamic loco-grasping and high-load capacities both in climbing and on the ground. The torso mechanisms allow SCALER to stretch the end-effector workspace on demand. The spine-enhanced GOAT grippers successfully support SCALER on the ceiling with slippery and rough surfaces. SCALER achieved dynamic climbing with the pneumatically actuated GOAT grippers, which was 13.8 times faster than the previous fastest SCALER climbing. With C-GOAT grippers, SCALER performs multi-modal grasping, thereby overcoming environments otherwise infeasible. SCALER has demonstrated versatility by traversing vertical and inverted walls and achieving comparable speeds to state-of-the-art robots on the ground. It exhibits one of the highest mechanical efficiency as a quadruped robot, showcasing its potential for broader applications and research. SCALER is one of the first to realize multi-modal grasping in free climbing. Hence, SCALER sets a new precedent for free-climbing robotics and advances the traversability of quadruped-limbed robots.

REFERENCES

- [1] K. Uno, N. Takada, T. Okawara, K. Haji, A. Candalot, W. F. R. Ribeiro *et al.*, "Hubrobo: A lightweight multi-limbed climbing robot for exploration in challenging terrain," in *2020 IEEE-RAS 20th International Conference on Humanoid Robots*, 2021, pp. 209–215.
- [2] M. Hutter, C. Gehring, D. Jud, A. Lauber, C. D. Bellicoso, V. Tsounis *et al.*, "AnyMal—a highly mobile and dynamic quadrupedal robot," in *2016 IEEE/RSJ international conference on intelligent robots and systems*. IEEE, 2016, pp. 38–44.
- [3] M. Sombolostan and Q. Nguyen, "Hierarchical adaptive loco-manipulation control for quadruped robots," *Proceedings 2023 IEEE/RSJ International Conference on Intelligent Robots and Systems*, 2022.
- [4] F. Shi, T. Homberger, J. Lee, T. Miki, M. Zhao, F. Farshidian *et al.*, "Circus anymal: A quadruped learning dexterous manipulation with its limbs," in *2021 IEEE International Conference on Robotics and Automation*. IEEE, 2021, pp. 2316–2323.
- [5] Z. Fu, X. Cheng, and D. Pathak, "Deep whole-body control: learning a unified policy for manipulation and locomotion," in *Conference on Robot Learning*. PMLR, 2023, pp. 138–149.
- [6] Y. Guan, L. Jiang, H. Zhu, X. Zhou, C. Cai, W. Wu *et al.*, "Climbot: A modular bio-inspired biped climbing robot," in *2011 IEEE/RSJ International Conference on Intelligent Robots and Systems*, 2011, pp. 1473–1478.
- [7] Y. Gong, G. Sun, A. Nair, A. Bidwai, R. CS, J. Grezmak *et al.*, "Legged robots for object manipulation: A review," *Frontiers in Mechanical Engineering*, vol. 9, 2023.
- [8] T. Bretl, "Motion planning of multi-limbed robots subject to equilibrium constraints: The free-climbing robot problem," *The International Journal of Robotics Research*, vol. 25, no. 4, pp. 317–342, 2006.
- [9] M. Kanazawa, S. Nozawa, Y. Kakiuchi, Y. Kanemoto, M. Kuroda, K. Okada *et al.*, "Robust vertical ladder climbing and transitioning between ladder and catwalk for humanoid robots," in *2015 IEEE/RSJ International Conference on Intelligent Robots and Systems*. IEEE, 2015, pp. 2202–2209.
- [10] P. Beal, *Bouldering: Movement, Tactics, and Problem Solving*. The Mountaineers Books, 2011.
- [11] C. Balaguer, A. Gimenez, and A. Jardón, "Climbing robots' mobility for inspection and maintenance of 3d complex environments," *Autonomous Robots*, vol. 18, pp. 157–169, 2005.
- [12] Y. Tanaka, Y. Shirai, X. Lin, A. Schperberg, H. Kato, A. Swardlow *et al.*, "Scaler: A tough versatile quadruped free-climber robot," in *2022 IEEE/RSJ International Conference on Intelligent Robots and Systems*, 2022, pp. 5632–5639.
- [13] S. Seok, A. Wang, M. Y. Chuah, D. Otten, J. Lang, and S. Kim, "Design principles for highly efficient quadrupeds and implementation on the mit cheetah robot," in *2013 IEEE International Conference on Robotics and Automation*. IEEE, 2013, pp. 3307–3312.
- [14] K. Weinmeister, P. Eckert, H. Witte, and A.-J. Ijspeert, "Cheetah-cub-s: Steering of a quadruped robot using trunk motion," in *2015 IEEE international symposium on safety, security, and rescue robotics (SSRR)*. IEEE, 2015, pp. 1–6.
- [15] M. Su, Y. Qiu, Y. Guan, H. Zhu, and Z. Liu, "Climbot-Ω: A soft robot with novel grippers and rigid-compliantly constrained body for climbing on various poles," in *2021 IEEE/RSJ International Conference on Intelligent Robots and Systems*. IEEE, 2021, pp. 4975–4981.
- [16] W. Haomachai, D. Shao, W. Wang, A. Ji, Z. Dai, and P. Manoonpong, "Lateral undulation of the bendable body of a gecko-inspired robot for energy-efficient inclined surface climbing," *IEEE Robotics and Automation Letters*, vol. 6, no. 4, pp. 7917–7924, 2021.
- [17] S. Hong, Y. Um, J. Park, and H.-W. Park, "Agile and versatile climbing on ferromagnetic surfaces with a quadrupedal robot," *Science Robotics*, vol. 7, no. 73, p. eadd1017, 2022.
- [18] A. Parness, N. Abcouwer, C. Fuller, N. Wiltse, J. Nash, and B. Kennedy, "Lemur 3: A limbed climbing robot for extreme terrain mobility in space," in *2017 IEEE international conference on robotics and automation*. IEEE, 2017, pp. 5467–5473.
- [19] K. Nagaoka, H. Minote, K. Maruya, Y. Shirai, K. Yoshida, T. Hakamada *et al.*, "Passive spine gripper for free-climbing robot in extreme terrain," *IEEE Robotics and Automation Letters*, vol. 3, no. 3, pp. 1765–1770, 2018.
- [20] G. Kenneally, A. De, and D. E. Koditschek, "Design principles for a family of direct-drive legged robots," *IEEE Robotics and Automation Letters*, vol. 1, no. 2, pp. 900–907, 2016.
- [21] N. Kau, A. Schultz, N. Ferrante, and P. Slade, "Stanford doggo: An open-source, quasi-direct-drive quadruped," in *2019 International conference on robotics and automation*. IEEE, 2019, pp. 6309–6315.
- [22] M. P. Austin, J. M. Brown, C. A. Young, and J. E. Clark, "Leg design to enable dynamic running and climbing on bobcat," in *2018 IEEE/RSJ International Conference on Intelligent Robots and Systems*. IEEE, 2018, pp. 3799–3806.
- [23] Y. Liu, S. Sun, X. Wu, and T. Mei, "A wheeled wall-climbing robot with bio-inspired spine mechanisms," *Journal of Bionic Engineering*, vol. 12, no. 1, pp. 17–28, 2015.
- [24] A. Saunders, D. I. Goldman, R. J. Full, and M. Buehler, "The rise climbing robot: body and leg design," in *Unmanned Systems Technology VIII*, vol. 6230. SPIE, 2006, pp. 401–413.
- [25] S. Kim, M. Spenko, S. Trujillo, B. Heyneman, D. Santos, and M. R. Cutkosky, "Smooth vertical surface climbing with directional adhesion," *IEEE Transactions on robotics*, vol. 24, no. 1, pp. 65–74, 2008.
- [26] Y. Sakuhara, H. Shimizu, and K. Ito, "Climbing soft robot inspired by octopus," in *2020 IEEE 10th International Conference on Intelligent Systems (IS)*. IEEE, 2020, pp. 463–468.
- [27] D. Pagano and D. Liu, "An approach for real-time motion planning of an inchworm robot in complex steel bridge environments," *Robotica*, vol. 35, no. 6, pp. 1280–1309, 2017.
- [28] K. H. Cho, H. M. Kim, Y. H. Jin, F. Liu, H. Moon, J. C. Koo *et al.*, "Inspection robot for hanger cable of suspension bridge: Mechanism design and analysis," *IEEE/ASME Transactions on mechatronics*, vol. 18, no. 6, pp. 1665–1674, 2013.
- [29] T. Bandyopadhyay, R. Steindl, F. Talbot, N. Kottege, R. Dungavell, B. Wood *et al.*, "Magnetobot: A versatile multi-limbed inspection robot," in *2018 IEEE/RSJ International Conference on Intelligent Robots and Systems (IROS)*. IEEE, 2018, pp. 2253–2260.
- [30] M. Adinehvand, E. Asadi, C. Y. Lai, H. Khayyam, K. Tan, and R. Hoseinnezhad, "Bogiebot: A climbing robot in cluttered confined space of bogies with ferrous metal surfaces," in *2021 IEEE/RSJ International Conference on Intelligent Robots and Systems*. IEEE, 2021, pp. 2459–2466.
- [31] Y. Yoshida and S. Ma, "Design of a wall-climbing robot with passive suction cups," in *2010 IEEE International Conference on Robotics and Biomimetics*. IEEE, 2010, pp. 1513–1518.

- [32] C. Prados, M. Hernando, E. Gambao, and A. Brunete, "Moclora—an architecture for legged-and-climbing modular bio-inspired robotic organism," *Biomimetics*, vol. 8, no. 1, 2023.
- [33] R. Zhang and J.-C. Latombe, "Capuchin: A free-climbing robot," *International Journal of Advanced Robotic Systems*, vol. 10, no. 4, p. 194, 2013.
- [34] X. Lin, H. Krishnan, Y. Su, and D. W. Hong, "Multi-limbed robot vertical two wall climbing based on static indeterminacy modeling and feasibility region analysis," in *2018 IEEE/RSJ International Conference on Intelligent Robots and Systems*. IEEE, 2018, pp. 4355–4362.
- [35] S. Kim, A. T. Asbeck, M. R. Cutkosky, and W. R. Provancher, "Spinybotii: climbing hard walls with compliant microspines," in *ICAR'05. Proceedings, 12th International Conference on Advanced Robotics, 2005*. IEEE, 2005, pp. 601–606.
- [36] P. Birkmeyer, A. G. Gillies, and R. S. Fearing, "Clash: Climbing vertical loose cloth," in *2011 IEEE/RSJ International Conference on Intelligent Robots and Systems*. IEEE, 2011, pp. 5087–5093.
- [37] Y. Shirai, X. Lin, Y. Tanaka, A. Mehta, and D. Hong, "Risk-aware motion planning for a limbed robot with stochastic gripping forces using nonlinear programming," *IEEE Robotics and Automation Letters*, vol. 5, no. 4, pp. 4994–5001, 2020.
- [38] T. Kato, K. Uno, and K. Yoshida, "A pin-array structure for gripping and shape recognition of convex and concave terrain profiles," in *2022 IEEE International Conference on Robotics and Biomimetics*, 2022, pp. 1365–1370.
- [39] J. Vaillant, A. Kheddar, H. Audren, F. Keith, S. Brossette, K. Kaneko *et al.*, "Vertical ladder climbing by the hrp-2 humanoid robot," in *2014 IEEE-RAS International Conference on Humanoid Robots*, 2014, pp. 671–676.
- [40] S. Wang, H. Jiang, T. Myung Huh, D. Sun, W. Ruotolo, M. Miller *et al.*, "Spinyhand: Contact load sharing for a human-scale climbing robot," *Journal of Mechanisms and Robotics*, vol. 11, no. 3, p. 031009, 2019.
- [41] K. Hauser, S. Wang, and M. R. Cutkosky, "Efficient equilibrium testing under adhesion and anisotropy using empirical contact force models," *IEEE Transactions on Robotics*, vol. 34, no. 5, pp. 1157–1169, 2018.
- [42] F. Xu, F. Meng, Q. Jiang, and G. Peng, "Grappling claws for a robot to climb rough wall surfaces: Mechanical design, grasping algorithm, and experiments," *Robotics and Autonomous Systems*, vol. 128, p. 103501, 2020.
- [43] K. Uno, Y. Koizumi, K. Haji, M. Keiff, S. Harms, W. F. Ribeiro *et al.*, "Non-periodic gait planning based on salient region detection for a planetary cave exploration robot," 2020.
- [44] Y. Shirai, X. Lin, A. Schperberg, Y. Tanaka, H. Kato, V. Vichathorn *et al.*, "Simultaneous contact-rich grasping and locomotion via distributed optimization enabling free-climbing for multi-limbed robots," in *2022 IEEE/RSJ International Conference on Intelligent Robots and Systems*. IEEE, 2022, pp. 13 563–13 570.
- [45] Y. Tanaka, Y. Shirai, Z. Lacey, X. Lin, J. Liu, and D. Hong, "An under-actuated whipleretree mechanism gripper based on multi-objective design optimization with auto-tuned weights," in *2021 IEEE/RSJ International Conference on Intelligent Robots and Systems*, 2021, pp. 6139–6146.
- [46] T. Feix, J. Romero, H.-B. Schmiedmayer, A. M. Dollar, and D. Kragic, "The grasp taxonomy of human grasp types," *IEEE Transactions on Human-Machine Systems*, vol. 46, no. 1, pp. 66–77, 2016.
- [47] M. Corsaro, S. Tellex, and G. Konidaris, "Learning to detect multi-modal grasps for dexterous grasping in dense clutter," in *2021 IEEE/RSJ International Conference on Intelligent Robots and Systems*, 2021, pp. 4647–4653.
- [48] A. Schperberg, Y. Tanaka, F. Xu, M. Menner, and D. Hong, "Real-to-sim: Predicting residual errors of robotic systems with sparse data using a learning-based unscented kalman filter," in *2023 20th International Conference on Ubiquitous Robots*, 2023, pp. 27–34.
- [49] C. Gosselin *et al.*, "Stiffness mapping for parallel manipulators," *IEEE transactions on Robotics and Automation*, vol. 6, no. 3, pp. 377–382, 1990.
- [50] R. Thakker, M. Paton, M. P. Strub, M. Swan, G. Daddi, R. Royce *et al.*, "Eels: Towards autonomous mobility in extreme terrain with a versatile snake robot with resilience to exteroception failures," in *2023 IEEE/RSJ International Conference on Intelligent Robots and Systems (IROS)*, 2023, pp. 9886–9893.
- [51] R. B. McGhee and A. A. Frank, "On the stability properties of quadruped creeping gaits," *Mathematical Biosciences*, vol. 3, pp. 331–351, 1968.
- [52] K. Yoneda, H. Iiyama, and S. Hirose, "Intermittent trot gait of a quadruped walking machine dynamic stability control of an omnidirectional walk," in *Proceedings of IEEE International Conference on Robotics and Automation*, vol. 4, 1996, pp. 3002–3007 vol.4.
- [53] S. Wang, H. Jiang, and M. R. Cutkosky, "Design and modeling of linearly-constrained compliant spines for human-scale locomotion on rocky surfaces," *The International Journal of Robotics Research*, vol. 36, no. 9, pp. 985–999, 2017.
- [54] A. Schperberg, Y. Shirai, X. Lin, Y. Tanaka, and D. Hong, "Adaptive force controller for contact-rich robotic systems using an unscented kalman filter," in *2023 IEEE-RAS 23rd International Conference on Humanoid Robots*, 2023.
- [55] E. Donlon, S. Dong, M. Liu, J. Li, E. Adelson, and A. Rodriguez, "Gelslim: A high-resolution, compact, robust, and calibrated tactile-sensing finger," 2018.
- [56] A. Schperberg, Y. Tanaka, S. Mowlavi, F. Xu, B. Balaji, and D. Hong, "Optistate: State estimation of legged robots using gated networks with transformer-based vision and kalman filtering," in *2024 IEEE International Conference on Robotics and Automation (ICRA)*, 2024, pp. 6314–6320.
- [57] C. Ott, R. Mukherjee, and Y. Nakamura, "Unified impedance and admittance control," in *2010 IEEE International Conference on Robotics and Automation*, 2010, pp. 554–561.
- [58] J. Di Carlo, P. M. Wensing, B. Katz, G. Bledt, and S. Kim, "Dynamic locomotion in the mit cheetah 3 through convex model-predictive control," in *2018 IEEE/RSJ international conference on intelligent robots and systems*. IEEE, 2018, pp. 1–9.
- [59] C. Dumas, S. Caro, S. Garnier, and B. Furet, "Joint stiffness identification of six-revolute industrial serial robots," *Robotics and Computer-Integrated Manufacturing*, vol. 27, no. 4, pp. 881–888, 2011, conference papers of Flexible Automation and Intelligent Manufacturing.
- [60] P. Biswal and P. K. Mohanty, "Development of quadruped walking robots: A review," *Ain Shams Engineering Journal*, vol. 12, no. 2, pp. 2017–2031, 2021.
- [61] W. Yuan, S. Dong, and E. H. Adelson, "Gelsight: High-resolution robot tactile sensors for estimating geometry and force," *Sensors*, vol. 17, no. 12, p. 2762, 2017.
- [62] Y. Wang, Z. wei Chen, H. Zu, X. Zhang, C. Mao, and Z. Wang, "Improvement of heavy load robot positioning accuracy by combining a model-based identification for geometric parameters and an optimized neural network for the compensation of nongeometric errors," *Complexity*, vol. 2020, p. 5896813, 2020.
- [63] Y. Shirai, D. K. Jha, A. U. Raghunathan, and D. Hong, "Tactile tool manipulation," in *2023 IEEE International Conference on Robotics and Automation (ICRA)*, 2023, pp. 12 597–12 603.
- [64] J.-P. Roberge, W. Ruotolo, V. Duchaine, and M. Cutkosky, "Improving industrial grippers with adhesion-controlled friction," *IEEE Robotics and Automation Letters*, vol. 3, no. 2, pp. 1041–1048, 2018.